Electronic Supplementary Information

Structure-property relationships for bis-diketopyrrolopyrrole molecules in organic photovoltaics

Qiang (Mike) Wang, Jacobus J. van Franeker, Bardo J. Bruijnaers, Martijn M. Wienk and René A. J. Janssen

The supporting information contains the general experimental procedures, the synthesis and characterization details of the bis-DPP molecules (Schemes S1-S3), the cyclic voltammograms (Fig. S1), the device optimization (Tables S1-S8), the *J*−*V* characteristics, EQE data, and TEM images of the optimized devices (Figs. S2-S10), AFM images (Figs. S11-S12) and the X-ray diffraction patterns (Figs. S13-S14) of the bis-DPP molecules.

Materials and Measurement

All synthetic procedures were performed under argon atmosphere. Commercial chemicals and dry solvents were used as received. [60]PCBM was purchased from Solenne BV. 3-(5-Bromothiophen-2-yl)-2,5-bis(2-ethylhexyl)-6-(thiophen-2-yl)-2,5-dihydropyrrolo[3,4-c]pyrrole-1,4-dione (**1**), [1] bromothiophen-2-yl)-2,5-bis(2-hexyldecyl)-6-(thiophen-2-yl)-2,5-dihydropyrrolo[3,4-c]pyrrole-1,4-dione (**2**),[1] and 3-(5-(benzo[b]thiophen-2-yl)thiophen-2-yl)-6-(5-bromothiophen-2-yl)-2,5-bis(2-ethylhexyl)pyrrolo[3,4-c]pyrrole-1,4-dione (**3**) [2] were synthesized according to literature procedures. 2,5-Bis(trimethylstannyl)thieno[3,2-b]thiophene (**4**), 2,6-bis(trimethylstannyl)dithieno[3,2-b:2',3'-d]thiophene (**5**), 2,6-bis(trimethylstannyl)benzo[1,2-b:4,5-b']dithiophene (**6**), (4,8-bis(5-(2-ethylhexyl)thiophen-2-yl)benzo[1,2-b:4,5-b']dithiophene-2,6-diyl)bis(trimethylstannane) (**7**), and (4,8-bis(4,5-dihexylthiophen-2-yl)benzo[1,2-b:4,5-b']dithiophene-2,6-diyl)bis(trimethylstannane) (**8**) were obtained from SunaTech Inc.

^{1}H-NMR spectra were recorded at 500 MHz mercury spectrometer with $CDCl_3$ as the solvent and tetramethylsilane (TMS) as the internal standard. Optical absorption spectra were recorded on a Perkin Elmer Lambda 900 UV/vis/nearIR spectrophotometer. Cyclic voltammetry was performed under an inert atmosphere with a scan rate of 0.1 V s^{-1} and 1 M tetrabutylammonium hexafluorophosphate in dichloromethane as the electrolyte. A platinum working electrode, a silver counter electrode and a silver wire coated with silver chloride (Ag/AgCl) quasi-reference electrode were used combined with Fc/Fc^+ as the internal standard.

AFM images were taken on a Veeco MultiMode atomic force microscope connected to a Nanoscope III controller operating in tapping mode using PPP-NCH-50 probes (Nanosensors). For TEM, films were floated from the PEDOT-covered indium-tin-oxide substrates on 200 square mesh copper grids. TEM was performed with a Tecnai G2 Sphera (FEI) operating at 200 kV. XRD was measured on a Bruker D2 Endeavor diffractometer using Cu Kα radiation with a wavelength of 0.15406 nm. Scans were done from 2 – 30 degrees (2θ) with scan speed of 1 seconds/step and increments of 0.025 degree/step. Samples for XRD were prepared by drop casting 100 μL of a 5 mg/ml small molecule solution in chloroform on to a glass substrate.

Photovoltaic devices were made by spin coating poly(ethylenedioxythiophene): poly(styrene sulfonate) (PEDOT:PSS) (Clevios P, VP AI 4083) onto pre-cleaned, patterned indium tin oxide (ITO) substrates (14 Ω per square) (Naranjo Substrates). The photoactive layers were deposited by spin coating a chloroform solution containing the bis-DPP molecule (typically 5 or 10 mg ml^{-1}), the appropriate amount of [60]PCBM and the co-solvent (either 1,8-diiodooctane (DIO), ortho-dichlorobenzene (*o*-DCB), or 1-chloronaphthalene (1-CN)). For layers that were thermally annealed, the glass substrates with the photoactive layer were placed on a hot plate inside a N_2-filled glovebox (< 1 ppm O_2 and < 1 ppm H_2O) at the temperatures and times indicated in the tables. For cells that were thermal annealed, this was done prior to depositing the metal contacts. To complete the devices, LiF (1 nm) and Al (100 nm) were deposited by vacuum evaporation at ~2×10^{-7} mbar as the back electrode. The active area of the cells was 0.09 cm^2. *J–V* characteristics were measured under ~100 mW cm^{-2} white light from a tungsten-halogen lamp filtered by a Schott GG385 UV filter and a Hoya LB 120 daylight filter, using a Keithley 2400 source meter. Short circuit currents under AM1.5G conditions were estimated from the spectral response and convolution with the solar spectrum. The spectral response was measured under simulated 1 sun operation conditions using bias light from a 532 nm solid state laser (Edmund Optics). Light from a 50 W tungsten halogen lamp (Osram64610) was used as probe light and modulated with a mechanical chopper before passing the monochromator (Oriel, Cornerstone 130) to select the wavelength. The response was recorded as the voltage over a 50 Ω resistance, using a lock-in amplifier (Stanford Research Systems SR 830). A calibrated Si cell was used as reference. The device was kept behind a quartz window in a nitrogen filled container. The thickness of the active layers in the photovoltaic devices was measured on a Veeco Dektak 150 profilometer.

Synthesis of bis-DPP molecules

The synthetic route to the bis-DPP molecules is shown in Schemes S1, S2 and S3.

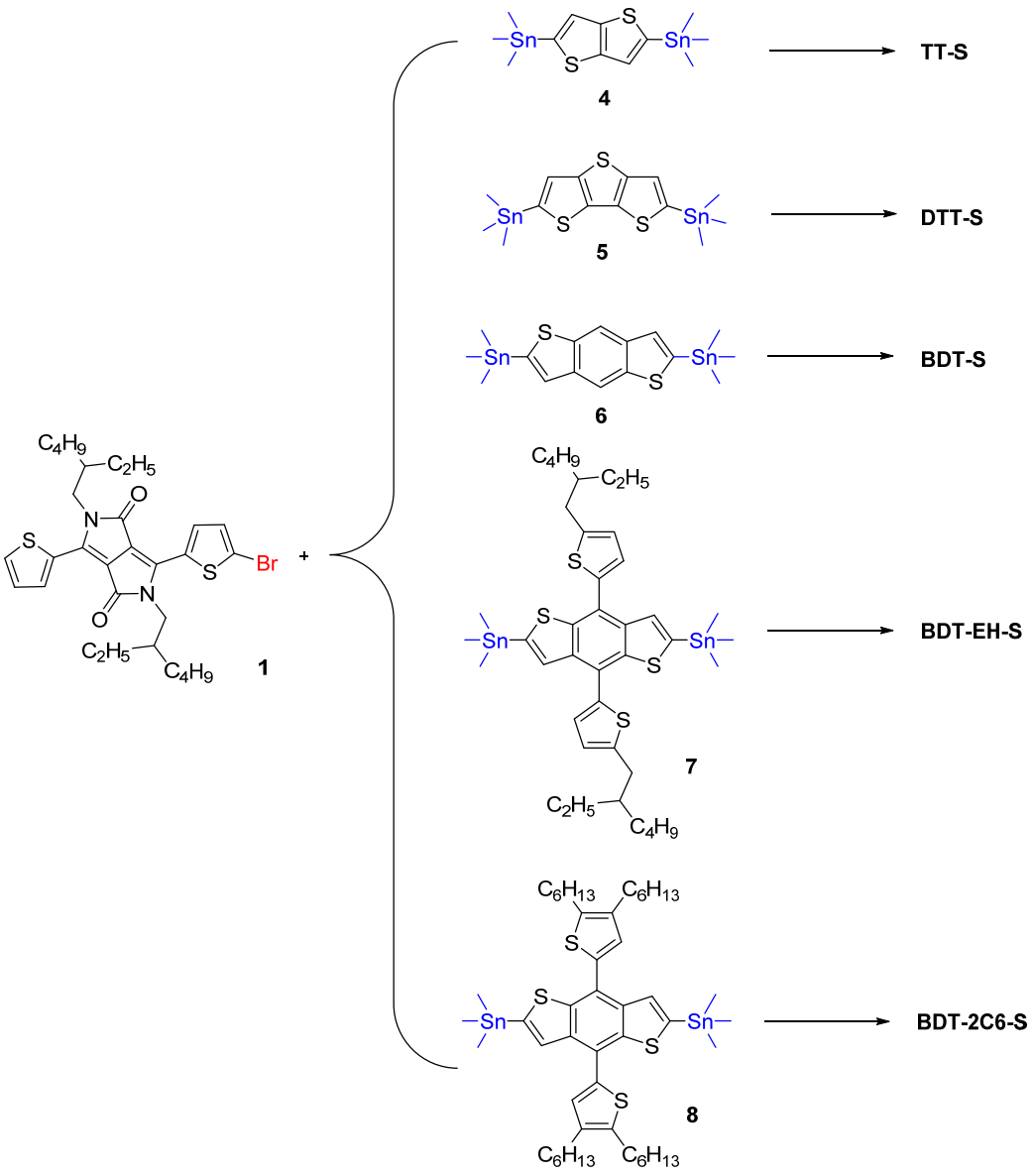

Scheme S1 Syntheses of bis-DPP-S molecules via Stille reaction using $Pd_2(dba)_3$ as catalyst in toluene at 115 °C.

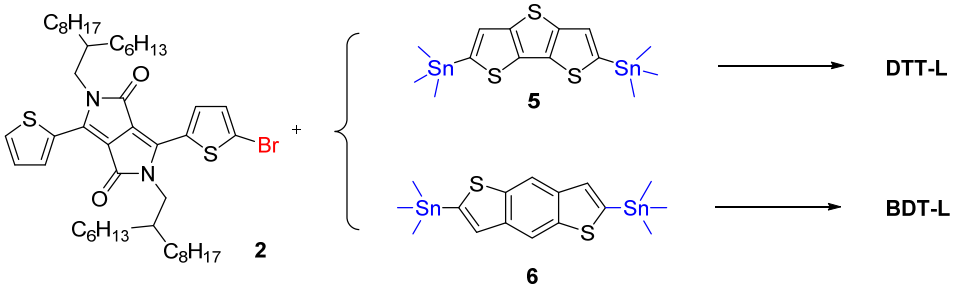

Scheme S2 Synthesis of DTT-L and BDT-L via Stille reaction using $Pd_2(dba)_3$ as catalyst in toluene at 115 °C.

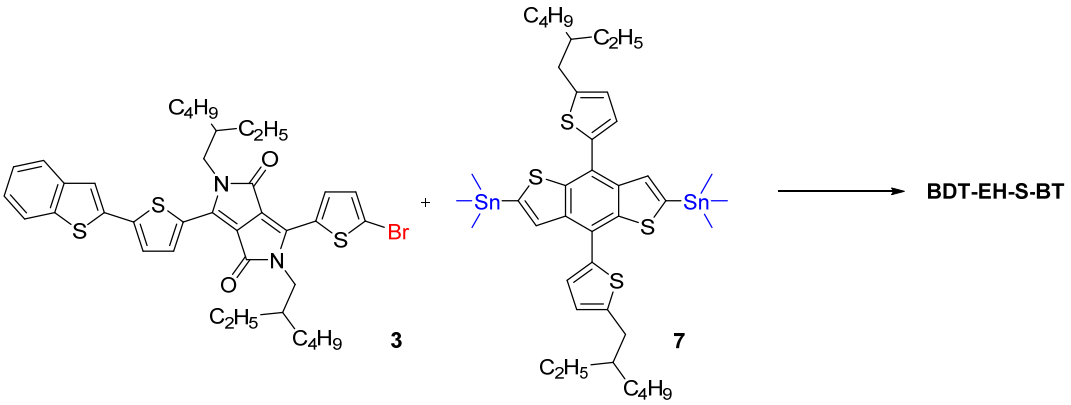

Scheme S3 Synthesis of BDT-EH-S-BT via Stille reaction using $Pd_2(dba)_3$ as catalyst in toluene at 115 °C.

General procedure for Stille reactions

TT-S

A Schlenk tube was filled with Br-DPP (**1**) (127 mg, 0.21 mmol), bistannyl thienothiophene (**4**) (47 mg, 0.1 mmol), toluene (2 mL) and DMF (0.2 mL). The solution was bubbled with argon for 10 minutes. Then tris(dibenzylideneacetone)dipalladium(0) (3 mg, 3 µmol) and triphenylphosphine (3 mg, 12 µmol) were added. After degassing and refilling with argon three times, the reaction mixture was stirred at 115 °C for 12 h. The mixture was then extracted with dichloromethane, washed with water and brine, dried with Na_2SO_4 and concentrated by evaporating the solvent. The resulting solid was subjected to column chromatography (silica, eluent heptane/CH_2Cl_2, 2:1 to 1:2) to isolate the crude product. The resulting solid was dissolved in chloroform (5 mL) and precipitated into methanol (100 mL) to yield TT-S (56 mg, 47 %) as a dark blue solid. ^{1}H NMR (500 MHz, chloroform-*d*) δ 8.94 (d, J = 4.2 Hz, 2H), 8.90 (d, J = 3.6 Hz, 2H), 7.63 (d, J = 4.9 Hz, 2H), 7.46 (s, 2H), 7.36 (d, J = 4.1 Hz, 2H), 4.05 (h, J = 7.9, 7.5 Hz, 8H), 1.90 (dt, J = 25.7, 5.1 Hz, 4H), 1.40 – 1.26 (m, 35H), 0.95 – 0.85 (m, 24H). MS (MALDI): calculated: 1184.45, found: 1184.46 (M^+).

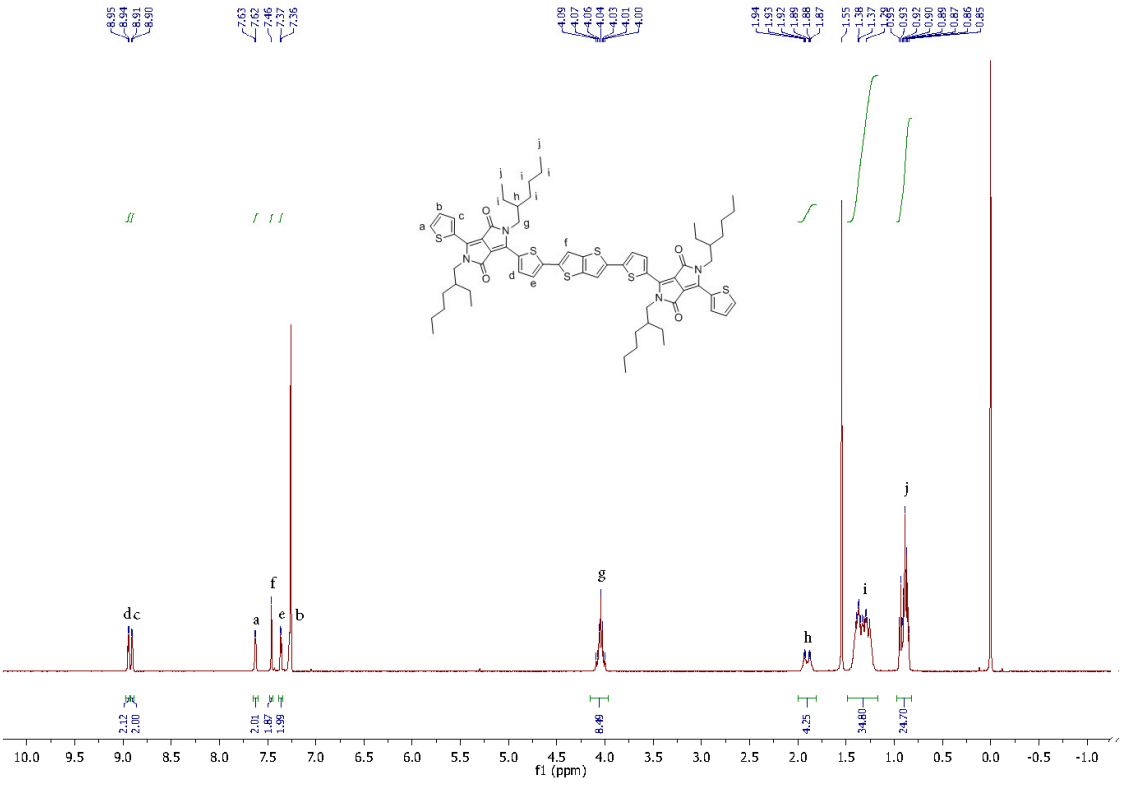

^{1}H NMR (500 MHz, chloroform-*d*) of TT-S.

DTT-S

The synthesis of DTT-S is similar to that of TT-S. DTT-S was isolated (62%) as a dark blue solid. ^{1}H NMR (500 MHz, chloroform-*d*) δ 8.95 (d, J = 4.2 Hz, 2H), 8.90 (d, J = 3.8 Hz, 2H), 7.61 (d, J = 4.9 Hz, 2H), 7.48 (s, 2H), 7.34 (d, J = 4.2 Hz, 2H), 4.13 – 3.95 (m, J = 7.7, 7.3 Hz, 8H), 1.94 – 1.85 (m, 4H), 1.47 – 1.19 (m, 36H), 0.95 – 0.85 (m, 26H). MS (MALDI): calculated: 1240.42, found: 1240.44 (M^+).

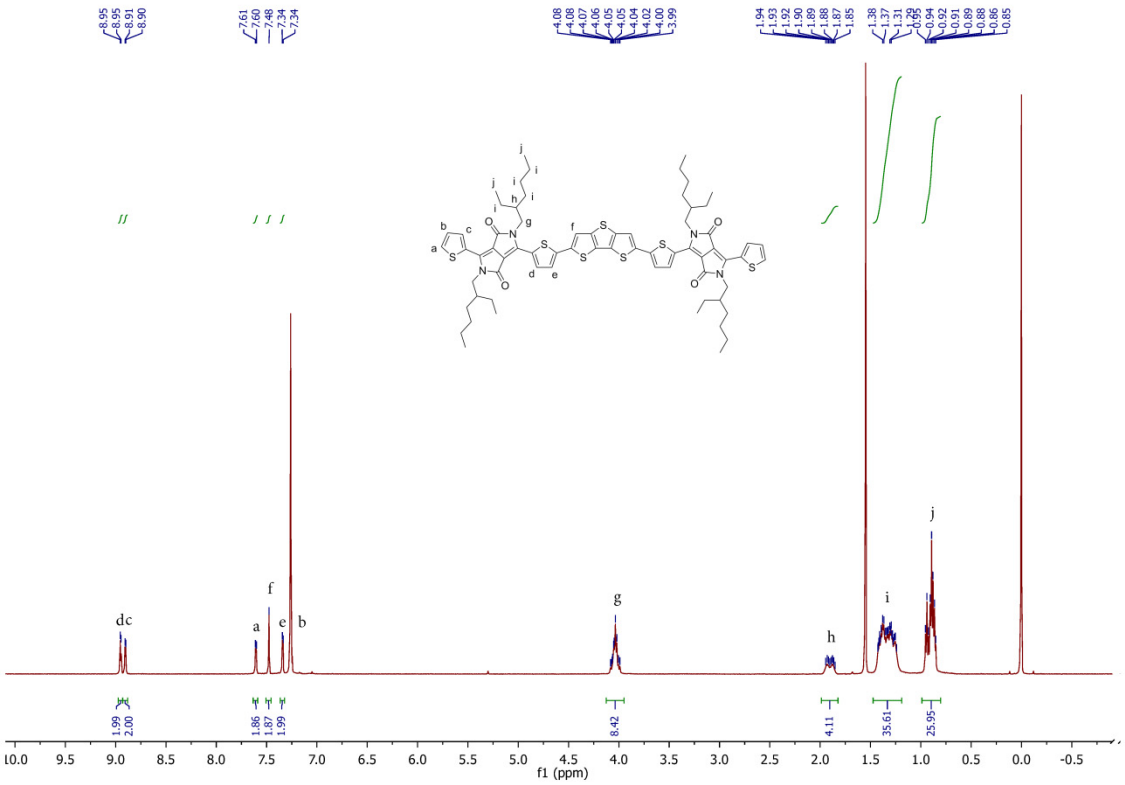

^{1}H NMR (500 MHz, chloroform-*d*) of DTT-S.

BDT-S

The synthesis of BDT-S is similar to that of TT-S. BDT-S was isolated (40%) as a dark blue solid. ^{1}H NMR (400 MHz, chloroform-*d*) δ 8.93 (d, J = 4.2 Hz, 2H), 8.91 (d, J = 3.9 Hz, 2H), 8.10 (s, 2H), 7.61 (d, J = 5.0 Hz, 2H), 7.50 (s, 2H), 7.41 (d, J = 4.2 Hz, 2H), 4.15 – 3.95 (m, 8H), 2.00 – 1.81 (m, 4H), 1.49 – 1.14 (m, 36H), 0.99 – 0.72 (m, 25H). MS (MALDI): calculated: 1234.47, found: (M^+) 1234.50.

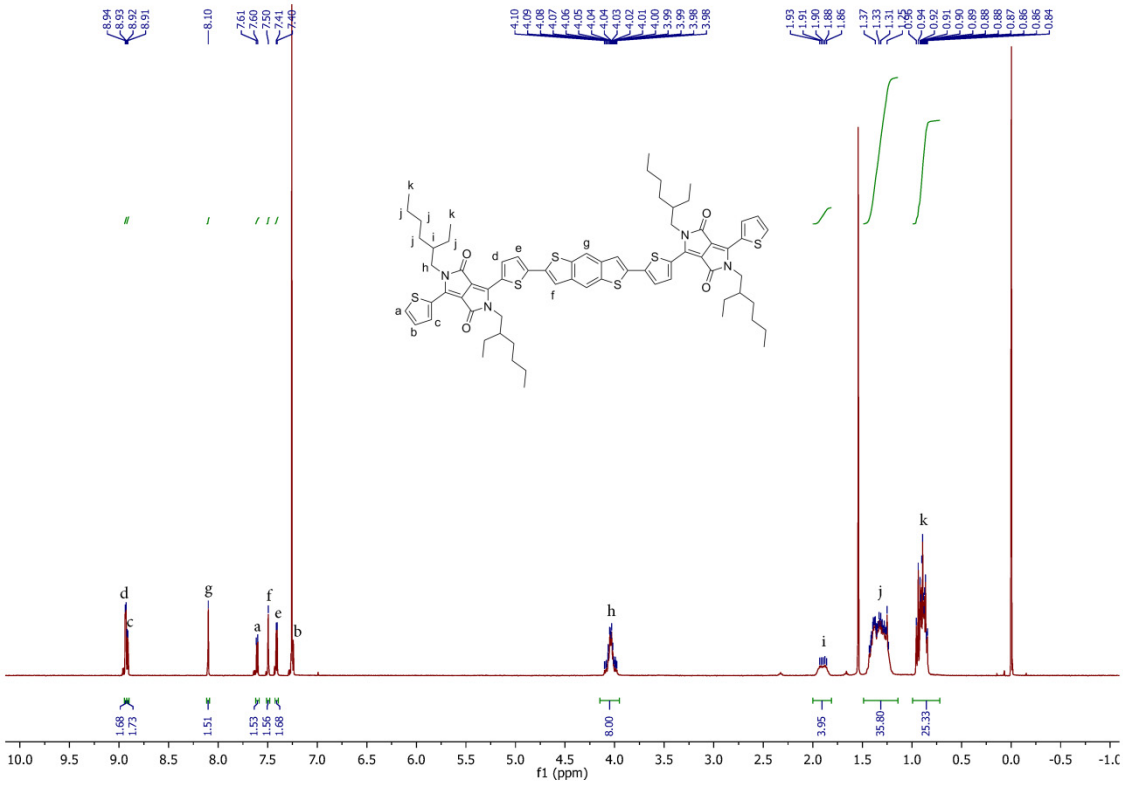

^{1}H NMR (500 MHz, chloroform-*d*) of BDT-S.

DTT-L

The synthesis of DTT-L is similar to that of TT-S. DTT-L was isolated (55%) as a dark blue solid. ^{1}H NMR (500 MHz, chloroform-*d*) δ 8.91 (d, J = 4.1 Hz, 2H), 8.88 (d, J = 3.6 Hz, 2H), 7.53 (d, J = 4.9 Hz, 2H), 7.36 (s, 2H), 7.23 (d, J = 4.1 Hz, 2H), 7.19 (t, J = 4.4 Hz, 2H), 4.03 – 3.97 (m, 8H), 1.96 – 1.90 (m, 4H), 1.46 – 1.13 (m, 98H), 0.85 (q, J = 6.5 Hz, 24H). MS (MALDI): calculated: 1688.92, found: (M^+) 1688.87.

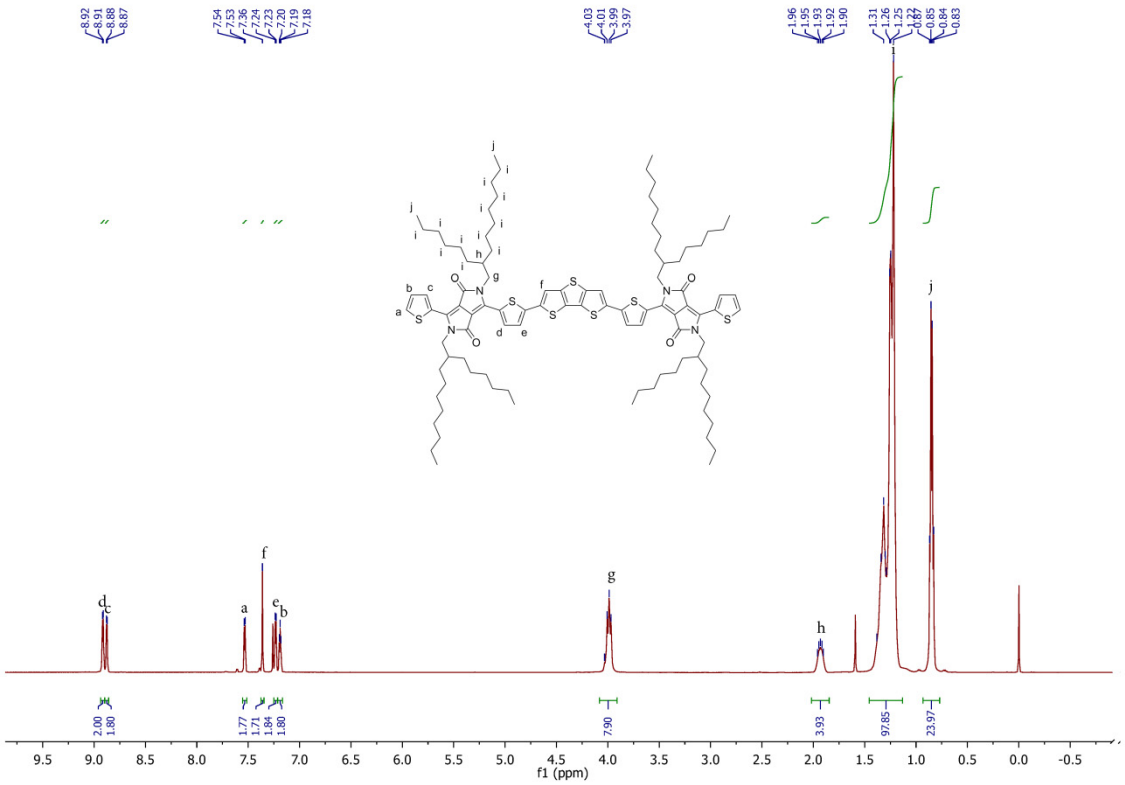

^{1}H NMR (500 MHz, chloroform-*d*) of DTT-L.

BDT-L

The synthesis of BDT-L is similar to that of TT-S. BDT-L was isolated (52%) as a dark blue solid. ^{1}H NMR (500 MHz, chloroform-*d*) δ 8.92 (d, J = 4.2 Hz, 2H), 8.90 (d, J = 4.0 Hz, 2H). 8.15 (s, 2H), 7.64 (d, J = 5.1 Hz, 2H), 7.57 (s, 2H), 7.46 (d, J = 5.0 Hz, 2H), δ 4.12 – 4.00 (m, 8H), 1.95 (d, J = 29.7 Hz, 4H), 1.46 – 1.13 (m, 101H), 0.87 – 0.82 (m, 24H). MS (MALDI): calculated: 1682.97, found: (M^+) 1682.98.

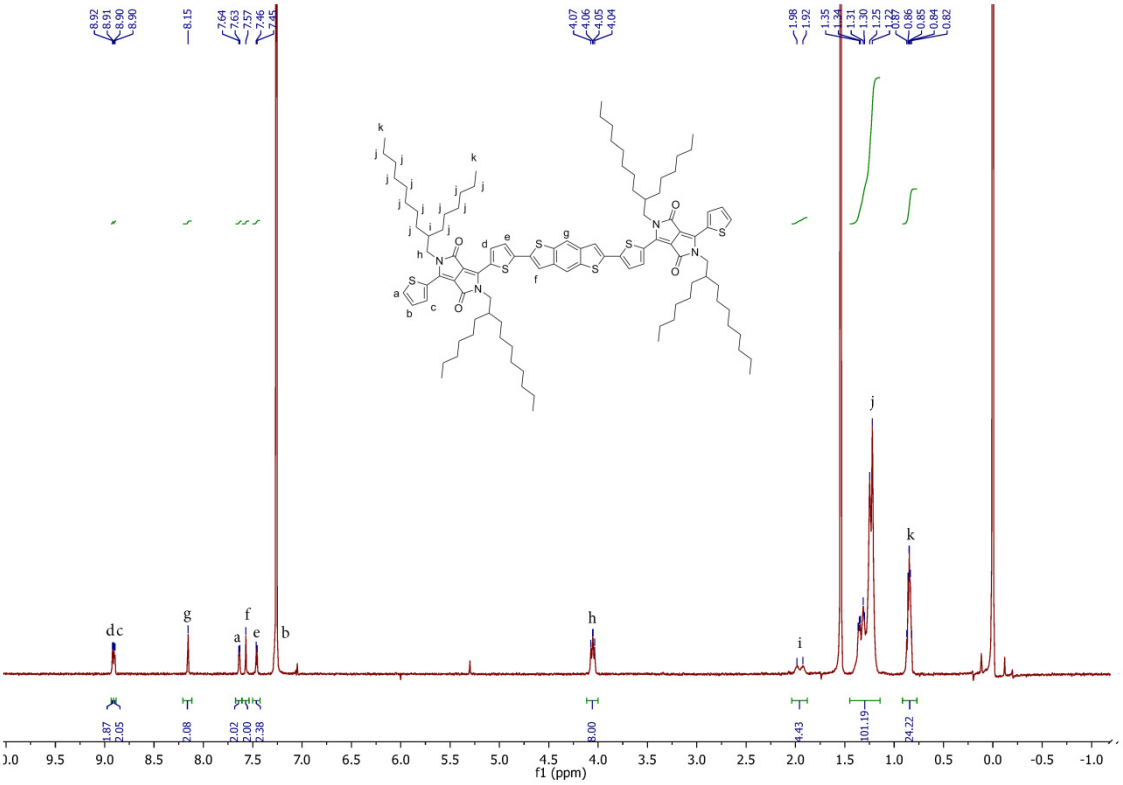

^{1}H NMR (500 MHz, chloroform-*d*) of BDT-L.

BDT-EH-S

The synthesis of BDT-EH-S is similar to that of TT-S. BDT-EH-S was isolated (59%) as a dark blue solid. ^{1}H NMR (500 MHz, chloroform-*d*) δ 8.94 (d, J = 4.0 Hz, 2H), δ 8.91 (d, J = 4.0 Hz, 2H), 7.77 (s, 2H), 7.60 (d, J = 5.0 Hz, 2H), 7.40 (d, J = 4.0 Hz, 2H), 7.36 (d, J = 4.0 Hz, 2H), 6.96 (d, J = 3.4 Hz, 2H), 4.03 (m, 8H), 2.92 (d, J = 6.8 Hz, 4H), 1.91 – 1.85 (m, 4H), 1.77 – 1.72 (m, 2H), 1.56 – 1.20 (m, 53H), 1.03 – 0.81 (m, 38H). MS (MALDI): calculated: 1622.69, found: (M^+) 1622.71.

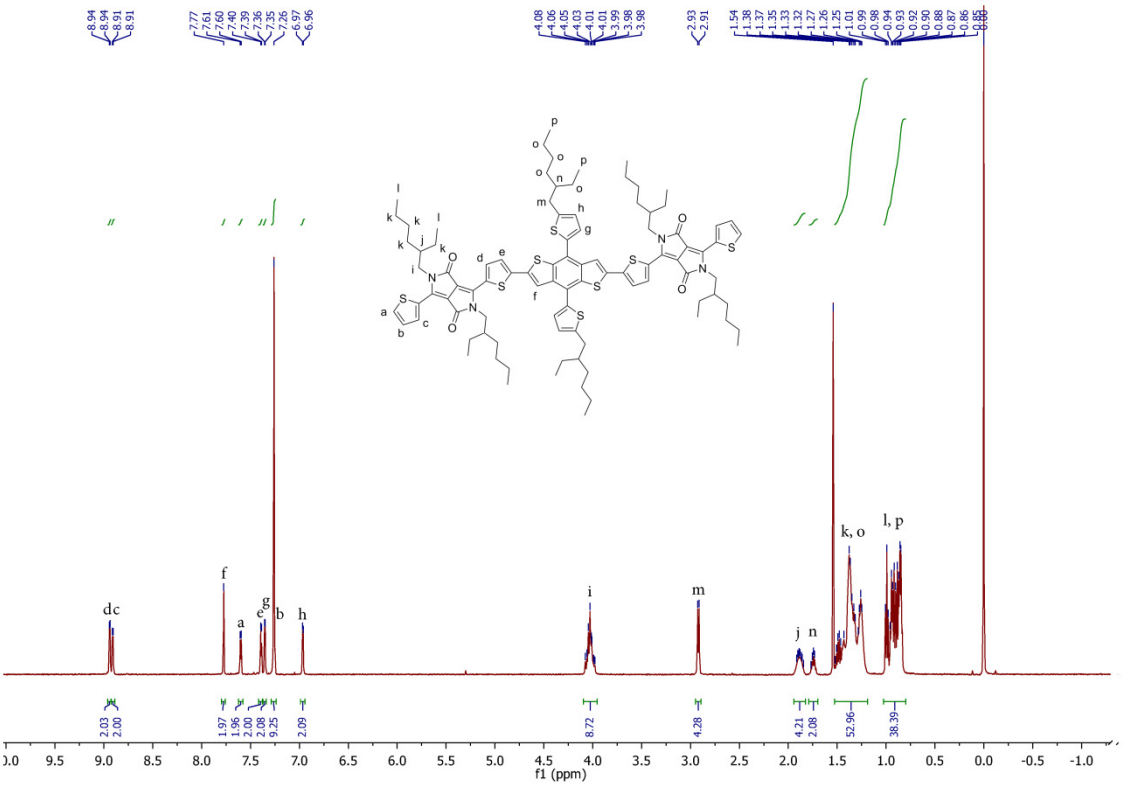

^{1}H NMR (500 MHz, chloroform-*d*) of BDT-EH-S.

BDT-2C6-S

The synthesis of BDT-2C6-S is similar to that of TT-S. BDT-2C6-S was isolated (61%) as a dark blue solid. ^{1}H NMR (500 MHz, chloroform-*d*) δ 8.93 (d, J = 4.1 Hz, 2H), 8.91 (d, J = 3.7 Hz, 2H), 7.85 (s, 2H), 7.63 (d, J = 4.9 Hz, 2H), 7.43 (d, J = 4.1 Hz, 2H), 7.28 (d, J = 4.2 Hz, 2H), 4.04 (m, 8H), 2.90 – 2.83 (m, 4H), 2.66 (m, 4H), 1.93 – 1.86 (m, 4H), 1.80 – 1.74 (m, 4H), 1.72 – 1.66 (m, 4H), 1.54 – 1.26 (m, 59H), 0.93 – 0.83 (m, 36H). MS (MALDI): calculated: 1734.82, found: (M^+) 1734.82.

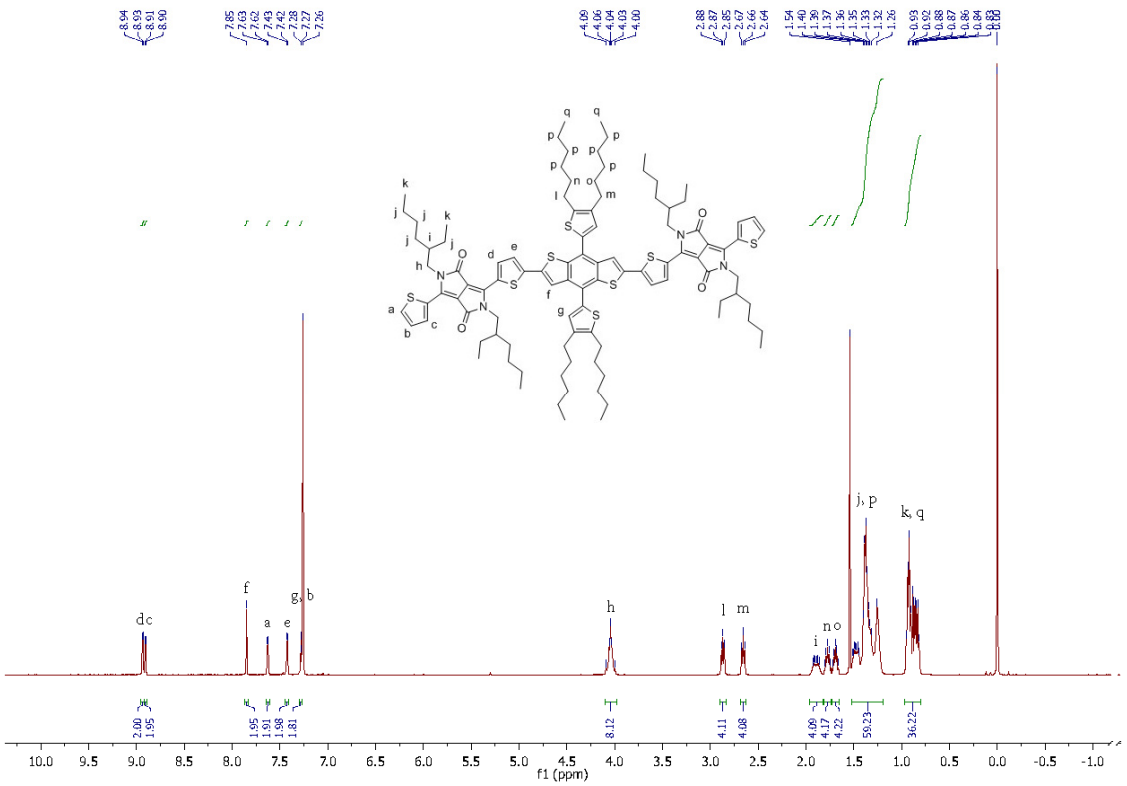

^{1}H NMR (500 MHz, chloroform-*d*) of BDT-2C6-S.

BDT-EH-S-BT

The synthesis of BDT-EH-S-BT is similar to that of TT-S. BDT-EH-S-BT was isolated (48%) as a dark blue solid. ^{1}H NMR (500 MHz, chloroform-*d*) δ 9.05 (d, J = 4.0 Hz, 2H), 8.97 (d, J = 4.1 Hz, 2H), 7.68 (d, J = 7.6 Hz, 2H), 7.65 (d, J = 7.6 Hz, 2H), 7.60 (s, 2H), 7.41 (d, 2H), 7.31 (d, 3H), 7.26 – 7.23 (m, 4H), 7.00 (d, J = 3.3 Hz, 2H), 3.97 (m, 9H), 2.97 (d, J = 6.9 Hz, 5H), 1.91 – 1.79 (m, 7H), 1.51 – 1.26 (m, 58H), 1.06 – 0.85 (m, 46H). MS (MALDI): calculated: 1886.70, found: (M^+) 1886.72.

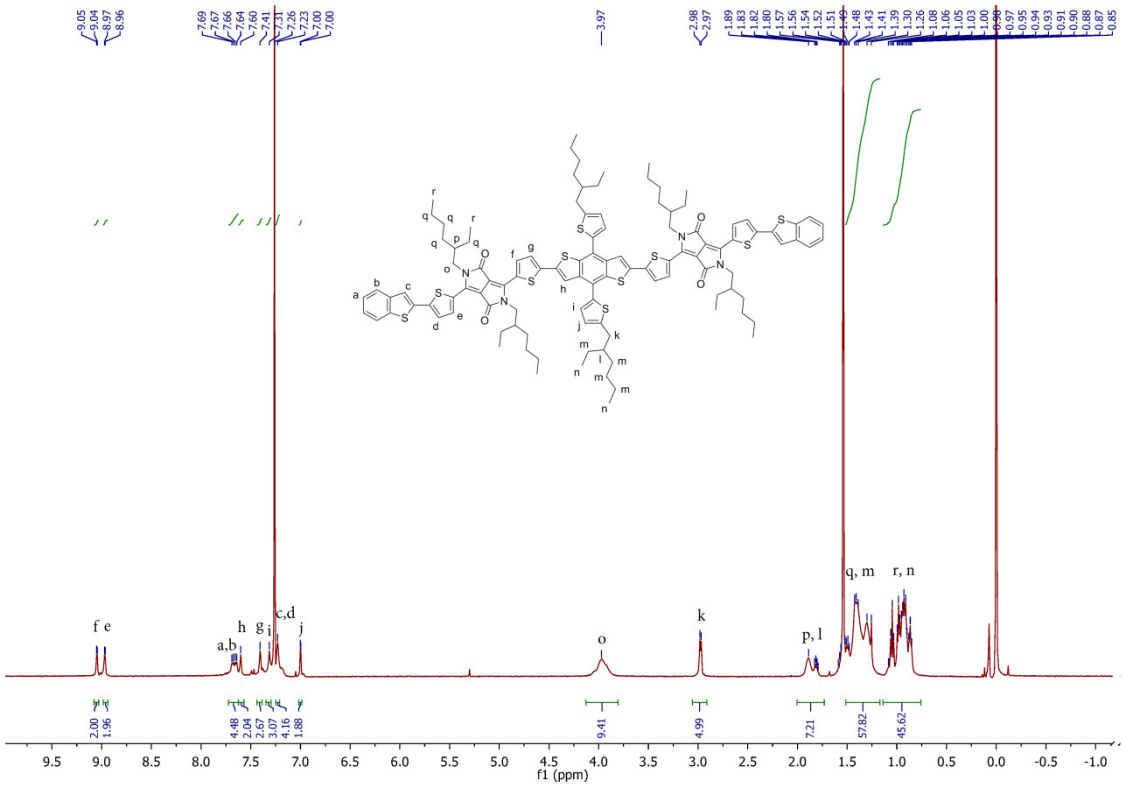

^{1}H NMR (500 MHz, chloroform-*d*) of BDT-EH-S-BT.

Cyclic voltammetry

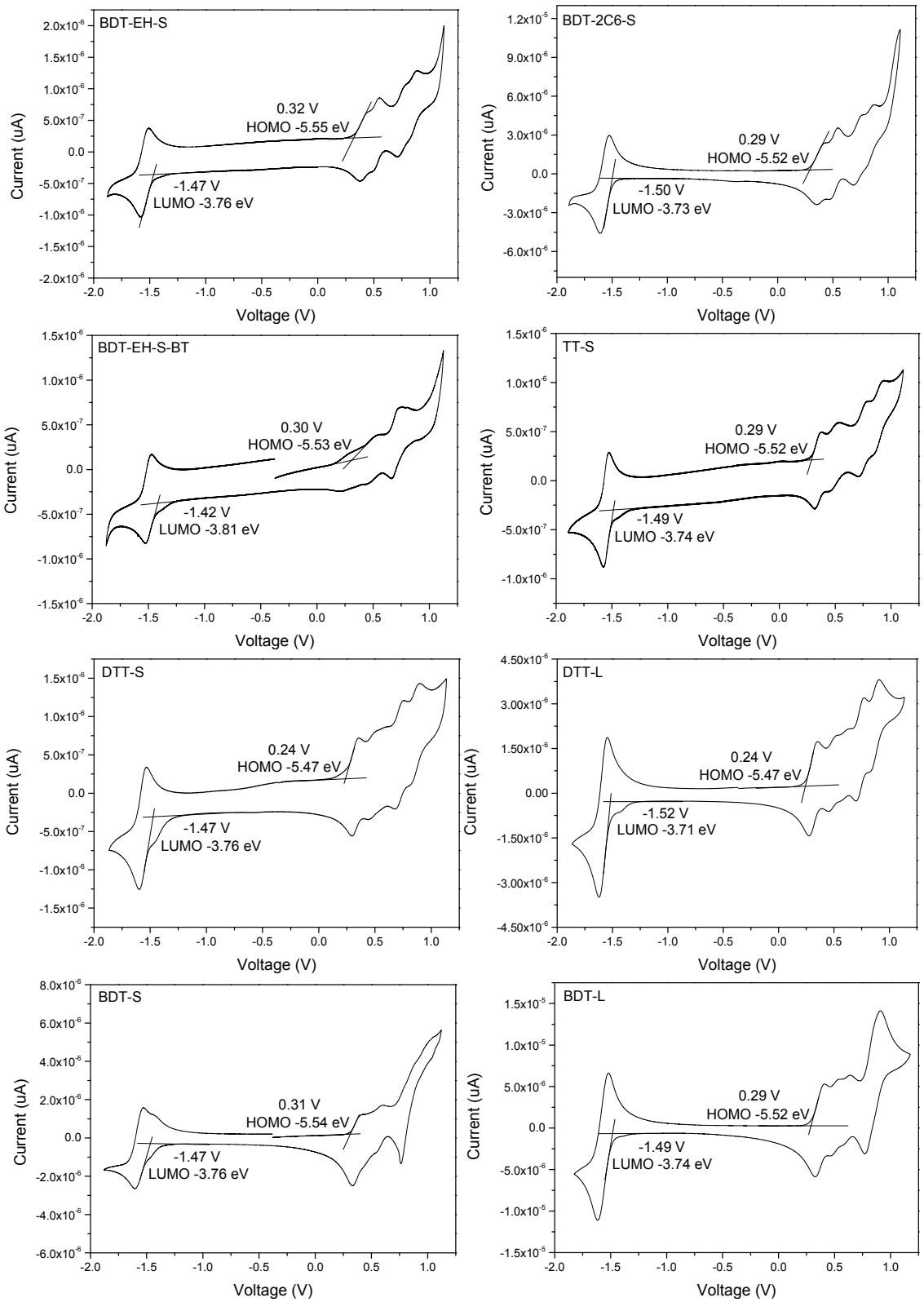

Fig. S1 Cyclic voltammograms of the DPP-based molecules in dichloromethane solution. Potential vs. Fc/Fc^{+}. (−5.23 eV vs. vacuum).

Results for TT-S:[60]PCBM

Table S1 Device parameters for TT-S:[60]PCBM [a]

D:A	Solvent	Annealing	J_{sc}	V_{oc}	FF	P	$J_{sc,sr}$[b]	PCE
1 : 1	$CHCl_3$	No	4.32	0.83	0.55	2.0		
1 : 1	$CHCl_3$	110 °C 10 min	6.21	0.84	0.55	2.9		
1 : 1	0.2% DIO/ $CHCl_3$	No	3.75	0.82	0.59	1.8		
1 : 1	0.2% DIO/ $CHCl_3$	110 °C 10 min	3.43	0.84	0.52	1.5		
1 : 1	0.2% o-DCB/ $CHCl_3$	110 °C 10 min	5.11	0.85	0.52	2.3		
1 : 1	0.2% 1-CN/ $CHCl_3$	No	8.66	0.78	0.57	3.9		
1 : 1	**0.2% 1-CN/ $CHCl_3$**	**110 °C 10 min**	**10.40**	**0.81**	**0.56**	**4.8**	**9.46**	**4.3**
2 : 1	0.2% 1-CN/ $CHCl_3$	110 °C 10 min	4.55	0.85	0.52	2.0		
1 : 2	0.2% 1-CN/ $CHCl_3$	110 °C 10 min	7.93	0.81	0.57	3.7		

[a] Units: J_{sc} (mA cm^{-2}), V_{oc} (V), P (mW cm^{-2}), $J_{sc,sr}$ (mA cm^{-2}), and PCE (%).
[b] Current density based on integration of EQE correction, measured with light bias.

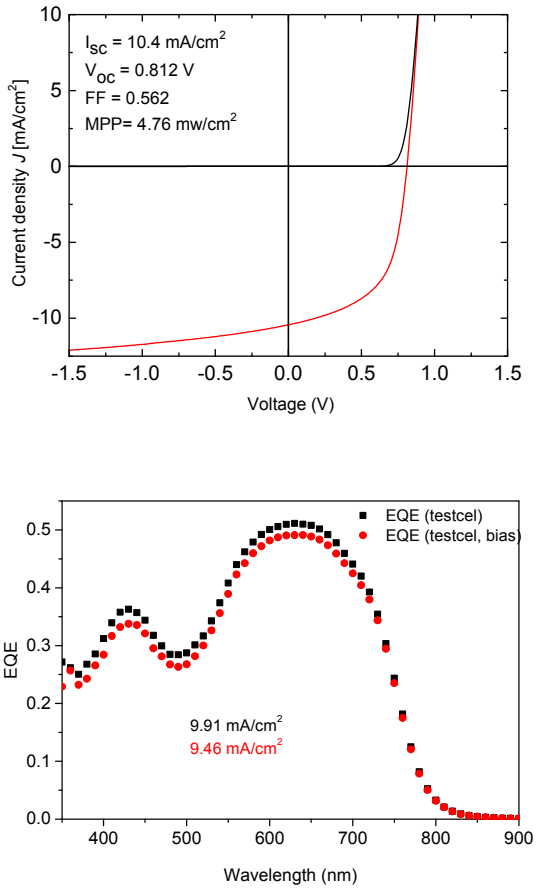

Fig. S2a TT-S:[60]PCBM *J-V* curve and EQE of optimized device

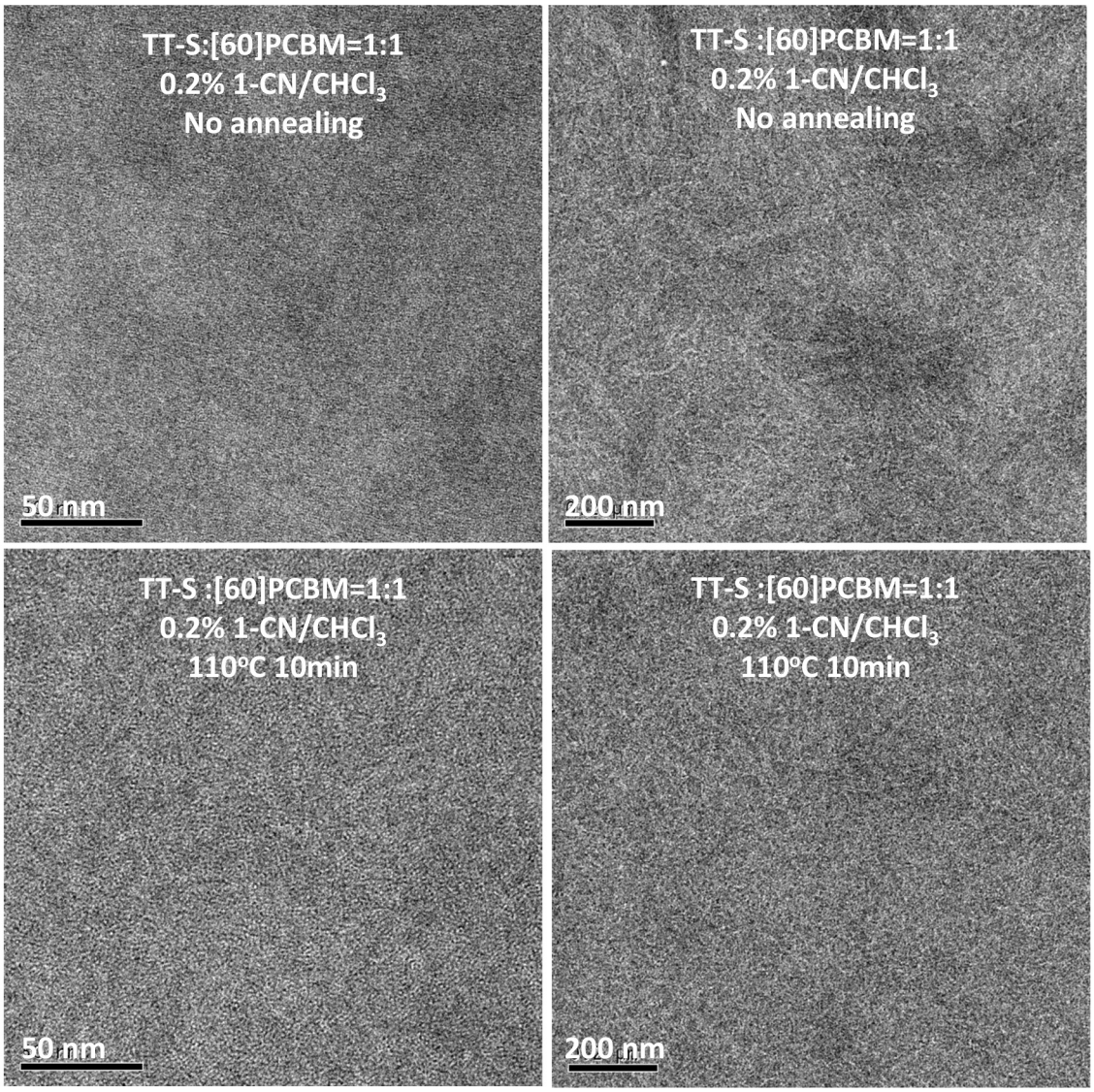

Fig. S2b. TEM images of optimized photoactive layers of TT-S:[60]PCBM before and after annealing.

Results for DTT-S:[60]PCBM

Table S2 Device parameters for DTT-S:[60]PCBM[a]

D:A	Solvent	Annealing	J_{sc}	V_{oc}	FF	P	$J_{sc,sr}$[b]	PCE
1 : 1	$CHCl_3$	No	6.74	0.75	0.45	2.24		
1 : 1	$CHCl_3$	110 °C 10 min	6.80	0.77	0.41	2.14		
1 : 1	0.2% DIO/ $CHCl_3$	No	5.69	0.71	0.44	1.78		
1 : 1	0.2% DIO/ $CHCl_3$	110 °C 10 min	6.77	0.68	0.33	1.52		
1 : 1	0.2% o-DCB/ $CHCl_3$	No	6.33	0.72	0.40	1.83		
1 : 1	0.2% o-DCB/ $CHCl_3$	110 °C 10 min	5.80	0.75	0.38	1.63		
1 : 1	0.1% 1-CN/ $CHCl_3$	No	5.22	0.84	0.52	2.26		
1 : 1	**0.2% 1-CN/ $CHCl_3$**	**No**	**7.49**	**0.76**	**0.44**	**2.47**	**6.82**	**2.3**
1 : 1	0.2% 1-CN/ $CHCl_3$	110 °C 10 min	4.44	0.67	0.36	1.06		
2 : 3	0.2% 1-CN/ $CHCl_3$	No	4.29	0.71	0.36	1.11		
3 : 2	0.2% 1-CN/ $CHCl_3$	No	4.08	0.77	0.39	1.22		
1 : 1	0.3% 1-CN/ $CHCl_3$	No	4.71	0.83	0.50	1.94		

[a] Units: J_{sc} (mA cm^{-2}), V_{oc} (V), P (mW cm^{-2}), $J_{sc,sr}$ (mA cm^{-2}), and PCE (%).
[b] Current density based on integration of EQE correction, measured with light bias.

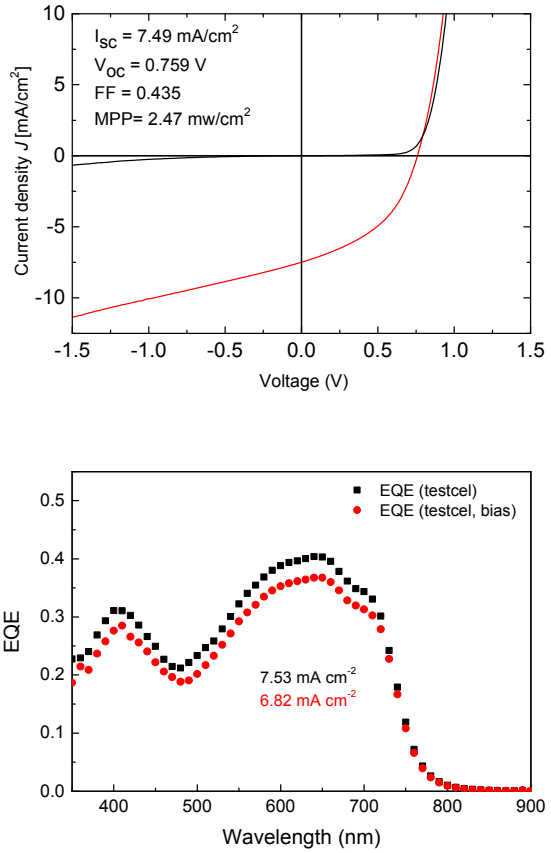

Fig. S3a DTT-S:[60]PCBM *J-V* curve and EQE of optimized device.

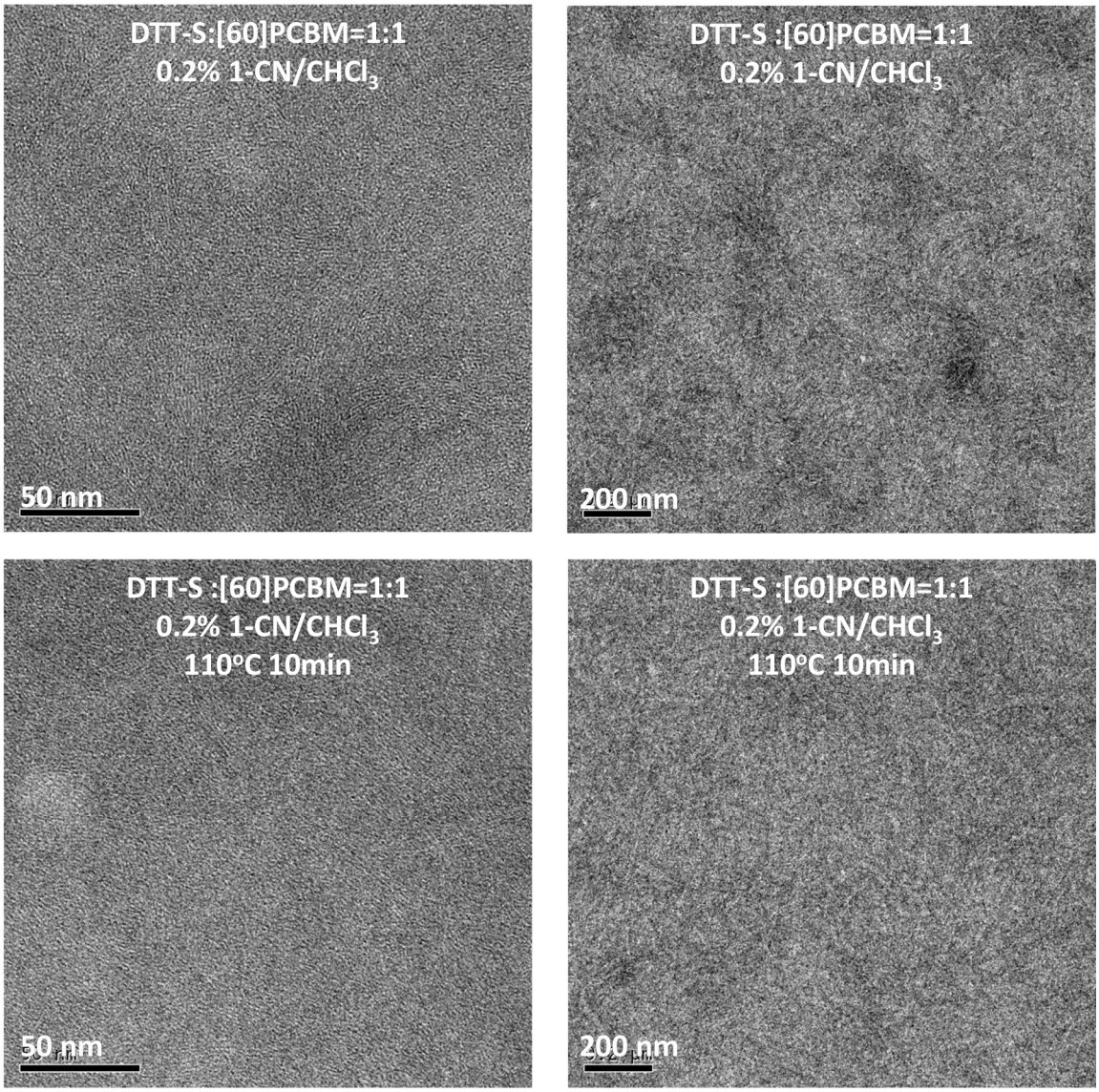

Fig. S3b. TEM images of optimized photoactive layers of DTT-S:[60]PCBM before and after annealing.

Results for BDT-S:[60]PCBM

Table S3 Device parameters for BDT-S:[60]PCBM[a]

D:A	Solvent	Annealing	J_{sc}	V_{oc}	FF	P	$J_{sc,sr}$ [b]	PCE
1 : 1	$CHCl_3$	No	3.71	0.802	0.573	1.70		
1 : 1	$CHCl_3$	110 °C 10 min	3.84	0.841	0.504	1.62		
1 : 1	0.2% DIO/ $CHCl_3$	No	3.71	0.804	0.486	1.45		
1 : 1	0.2% DIO/ $CHCl_3$	110 °C 10 min	3.57	0.820	0.427	1.25		
1 : 1	0.5% *o*-DCB/ $CHCl_3$	No	3.35	0.801	0.477	1.28		
1 : 1	0.5% *o*-DCB/ $CHCl_3$	110 °C 10 min	3.25	0.827	0.454	1.22		
1 : 1	0.1% 1-CN/ $CHCl_3$	No	3.28	0.908	0.312	0.93		
1 : 1	**0.2% 1-CN/ $CHCl_3$**	**No**	**6.06**	**0.846**	**0.530**	**2.72**	**5.95**	**2.67**
1 : 1	0.2% 1-CN/ $CHCl_3$	110 °C 10 min	4.66	0.832	0.455	1.77		
1 : 1	0.3% 1-CN/ $CHCl_3$	No	5.39	0.849	0.560	2.56		

[a] Units: J_{sc} (mA cm^{-2}), V_{oc} (V), P (mW cm^{-2}), $J_{sc,sr}$ (mA cm^{-2}), and PCE (%).
[b] Current density based on integration of EQE correction, measured with light bias.

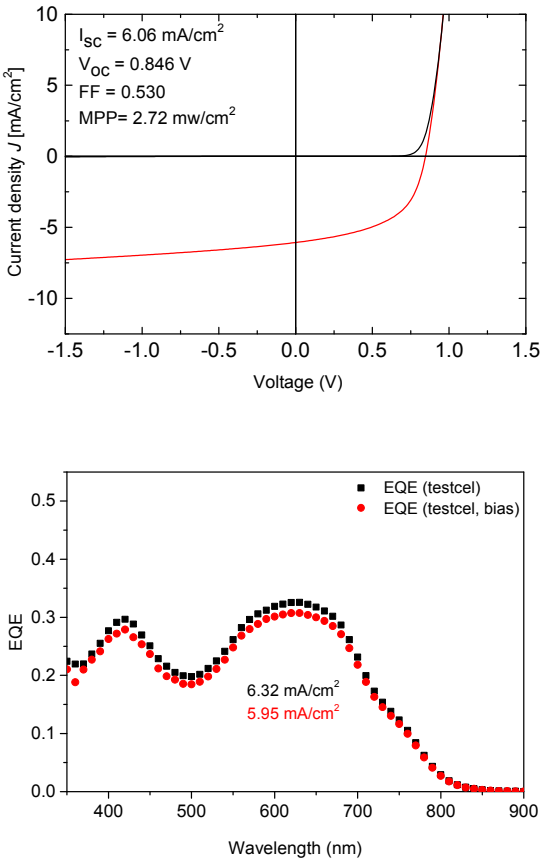

Fig. S4a BDT-S:[60]PCBM *J-V* curve and EQE of optimized device.

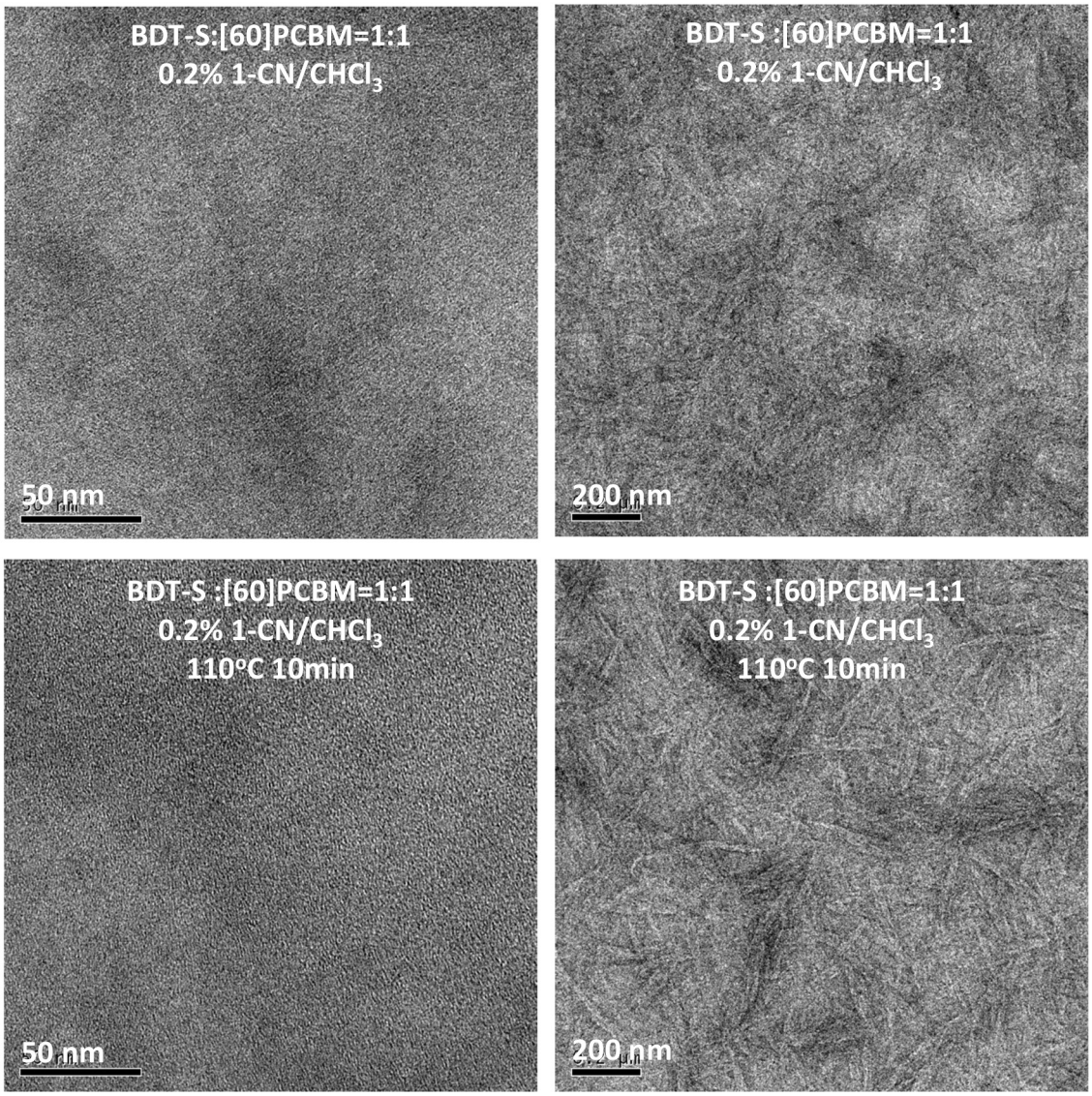

Fig. S4b. TEM images of optimized photoactive layers of BDT-S:[60]PCBM before and after annealing.

Results for DTT-L:[60]PCBM

Table S4 Device parameters for DTT-L:[60]PCBM[a]

D:A	Solvent	Annealing	J_{sc}	V_{oc}	FF	P	$J_{sc,sr}$[b]	PCE
1 : 1	$CHCl_3$	No	2.06	0.817	0.645	1.09		
1 : 1	$CHCl_3$	110 °C 10 min	1.74	0.813	0.510	0.72		
1 : 1	0.2% DIO/ $CHCl_3$	No	2.50	0.814	0.601	1.22		
1 : 1	0.2% DIO/$CHCl_3$	110 °C 10 min	2.40	0.829	0.547	1.09		
1 : 1	0.2% *o*-DCB/$CHCl_3$	No	3.16	0.825	0.637	1.66		
1 : 1	0.2% *o*-DCB/$CHCl_3$	110 °C 10 min	2.33	0.827	0.533	1.03		
1 : 1	0.1% 1-CN/$CHCl_3$	No	4.01	0.819	0.582	1.91		
1 : 1	**0.2% 1-CN/$CHCl_3$**	**No**	**5.38**	**0.806**	**0.602**	**2.61**	**5.83**	**2.83**
1 : 1	0.2% 1-CN/ $CHCl_3$	110 °C 10 min	3.30	0.838	0.594	1.64		
1:1.5	0.2% 1-CN/$CHCl_3$	No	4.87	0.812	0.598	2.36		
1 : 2	0.2% 1-CN/$CHCl_3$	No	4.10	0.810	0.598	1.98		
1 : 1	0.2% 1-CN/$CHCl_3$	110 °C 1 min	2.82	0.829	0.575	1.34		
1 : 1	0.2% 1-CN/$CHCl_3$	110 °C 3 min	2.95	0.831	0.570	1.40		
1 : 1	0.2% 1-CN/$CHCl_3$	110 °C 5 min	2.79	0.824	0.550	1.27		
1 : 1	0.2% 1-CN/$CHCl_3$	110 °C 7 min	3.38	0.830	0.567	1.59		
1 : 1	0.3% 1-CN/$CHCl_3$	No	4.79	0.800	0.623	2.39		

[a] Units: J_{sc} (mA cm^{-2}), V_{oc} (V), P (mW cm^{-2}), $J_{sc,sr}$ (mA cm^{-2}), and PCE (%).
[b] Current density based on integration of EQE correction, measured with light bias.

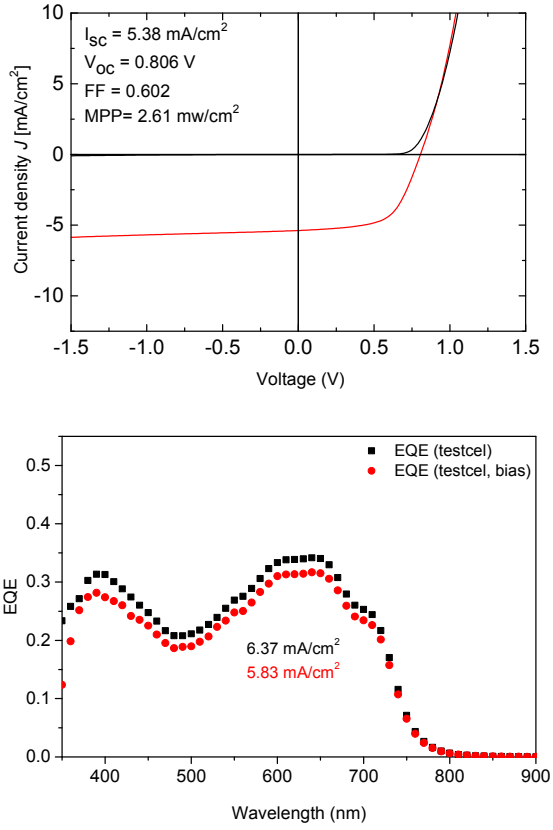

Fig. S5a DTT-L:[60]PCBM *J-V* curve and EQE of optimized device

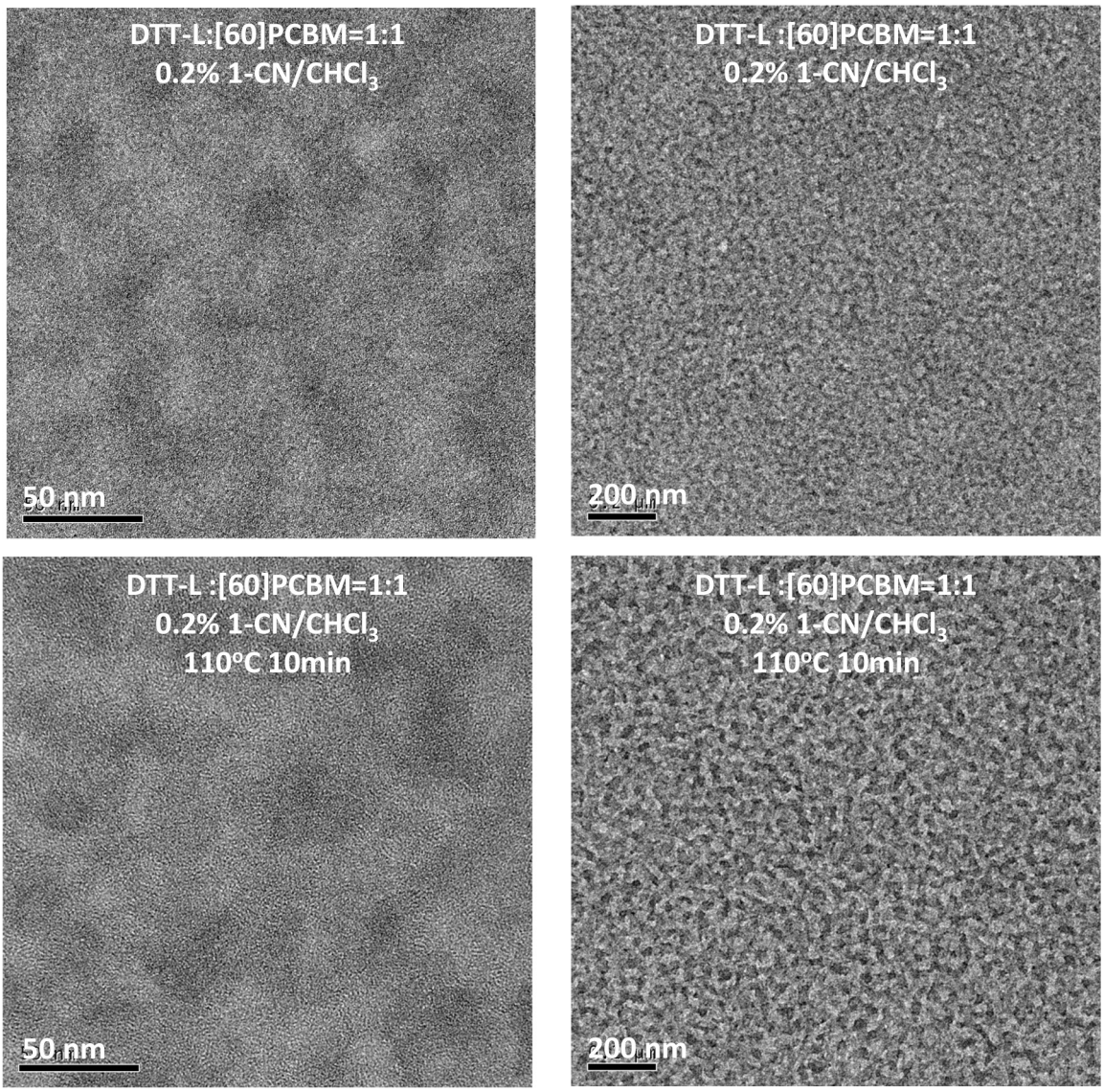

Fig. S5b. TEM images of optimized photoactive layers of DTT-L:[60]PCBM before and after annealing.

Results for BDT-L:[60]PCBM

Table S5 Device parameters for BDT-L:[60]PCBM[a]

D:A	Solvent	Annealing	J_{sc}	V_{oc}	FF	P	$J_{sc,sr}$[b]	PCE
1 : 1	$CHCl_3$	No	1.33	0.85	0.62	0.70		
1 : 1	$CHCl_3$	100 °C 5 min	1.96	0.89	0.47	0.82		
1 : 1	DIO: $CHCl_3$ 0.2%	No	1.61	0.84	0.63	0.86		
1 : 1	DIO: $CHCl_3$ 0.2%	100 °C 5 min	2.36	0.92	0.53	1.16		
1 : 1	*o*-DCB: $CHCl_3$ 0.2%	No	1.58	0.84	0.60	0.79		
1 : 1	*o*-DCB: $CHCl_3$ 0.2%	100 °C 5 min	2.36	0.93	0.52	1.14		
1 : 1	**1-CN: $CHCl_3$ 0.2%**	**No**	**4.68**	**0.85**	**0.58**	**2.31**	**5.53**	**2.73**
1 : 1	1-CN: $CHCl_3$ 0.2%	100 °C 5 min	4.01	0.90	0.52	1.86		

[a] Units: J_{sc} (mA cm^{-2}), V_{oc} (V), P (mW cm^{-2}), $J_{sc,sr}$ (mA cm^{-2}), and PCE (%).
[b] Current density based on integration of EQE correction, measured with light bias.

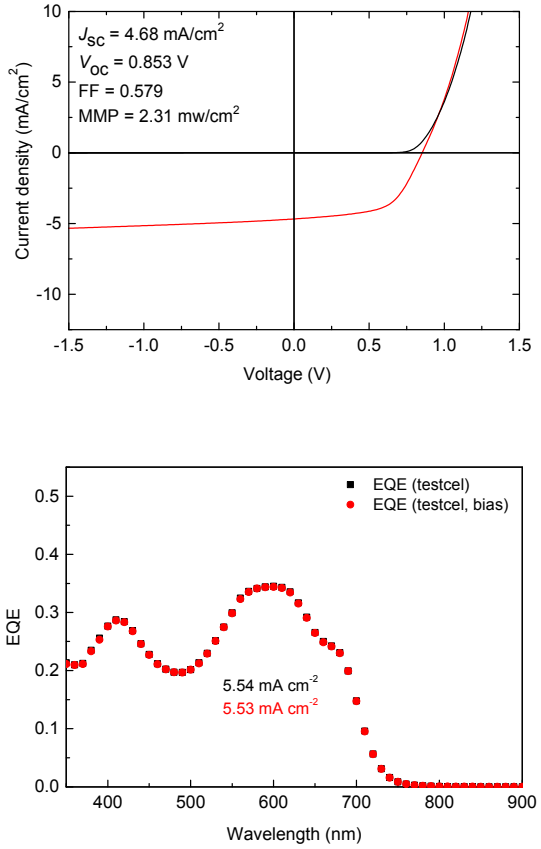

Fig. S6a BDT-L:[60]PCBM *J-V* curve and EQE of optimized device

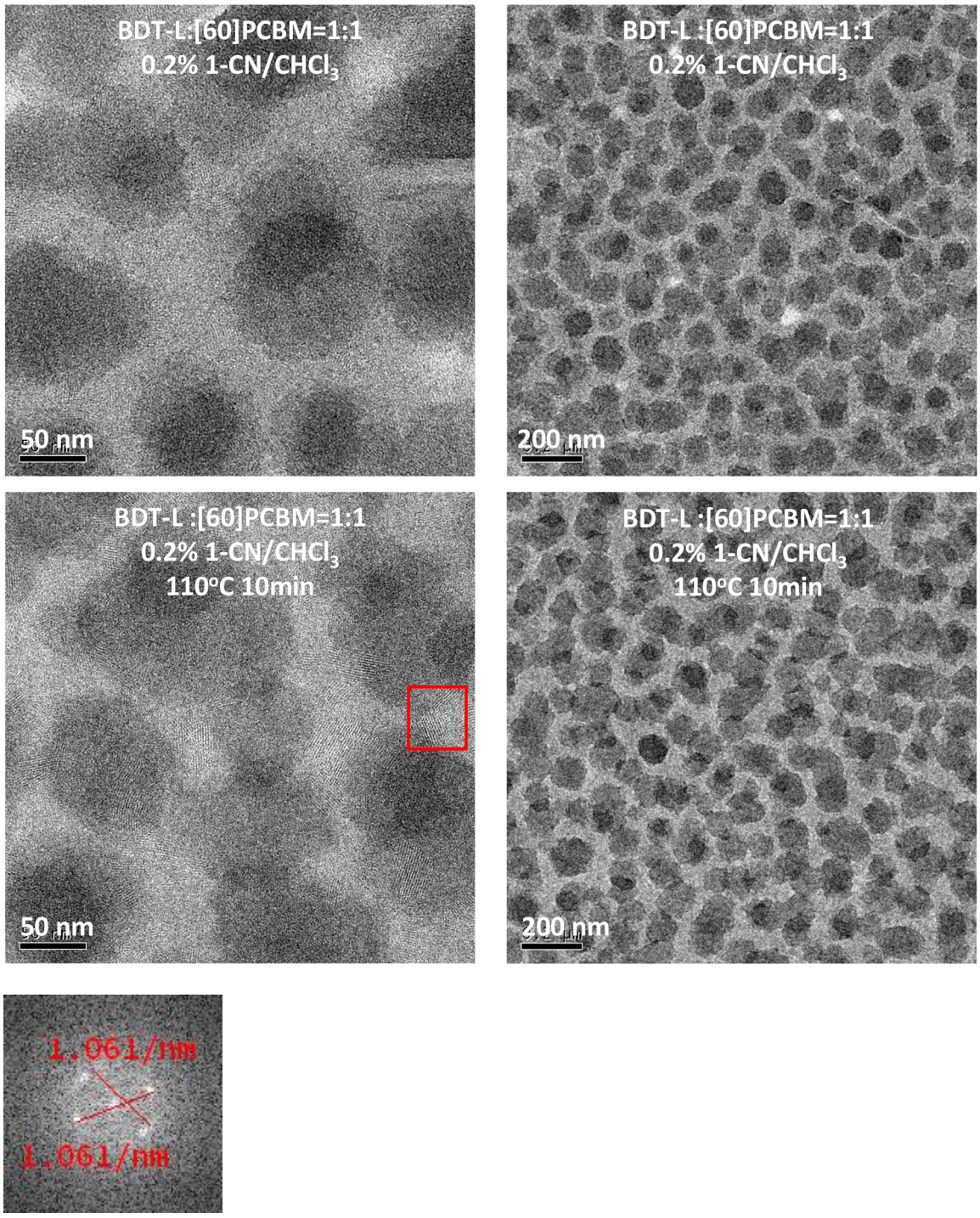

Fig. S6b TEM images of optimized photoactive layers of BDT-L:[60]PCBM before and after annealing. The lower image is a Fourier transform of the TEM image of the annealed blend showing the crystalline *d*-spacing of the BDT-L crystallites of 2/1.061 = 1.9 ± 0.1 nm.

Results for BDT-EH-S:[60]PCBM

Table S6 Device parameters for BDT-EH-S:[60]PCBM[a]

D:A	Solvent	Annealing	J_{sc}	V_{oc}	FF	P	$J_{sc,sr}$ [b]	PCE
1 : 1	$CHCl_3$	No	6.14	0.807	0.512	2.54		
1 : 1	$CHCl_3$	90 °C 10 min	9.87	0.830	0.558	4.58	8.83	4.09
1 : 1	**$CHCl_3$**	**110 °C 10 min**	**8.80**	**0.830**	**0.588**	**4.29**	**8.77**	**4.28**
1 : 1	$CHCl_3$	130 °C 10 min	5.58	0.802	0.524	2.35		
1 : 2	$CHCl_3$	110 °C 10 min	6.28	0.829	0.529	2.75		
2 : 1	$CHCl_3$	110 °C 10 min	7.70	0.825	0.426	2.71		
1 : 1	0.1% DIO/ $CHCl_3$	110 °C 10 min	10.20	0.832	0.531	4.48	8.95	3.95
1 : 1	0.2% DIO/ $CHCl_3$	No	9.44	0.862	0.432	3.52	8.11	3.02
1 : 1	0.3% DIO/ $CHCl_3$	No	8.01	0.781	0.569	3.55		
1 : 1	0.3% DIO/ $CHCl_3$	110 °C 10 min	7.18	0.832	0.573	3.42		
1 : 1	0.5% DIO/ $CHCl_3$	No	10.40	0.769	0.549	4.38	8.80	3.72
1 : 1	0.5% DIO/ $CHCl_3$	110 °C 10 min	8.05	0.828	0.587	3.91		
1 : 1	0.5% *o*-DCB/ $CHCl_3$	No	9.25	0.864	0.431	3.44		
1 : 1	0.2% 1-CN/ $CHCl_3$	No	7.01	0.916	0.388	2.49	6.76	2.40
1 : 1	**0.2% 1-CN/ $CHCl_3$**	**110 °C 10 min**	**9.15**	**0.829**	**0.564**	**4.28**	**9.36**	**4.38**

[a] Units: J_{sc} (mA cm^{-2}), V_{oc} (V), P (mW cm^{-2}), $J_{sc,sr}$ (mA cm^{-2}), and PCE (%).
[b] Current density based on integration of EQE correction, measured with light bias.

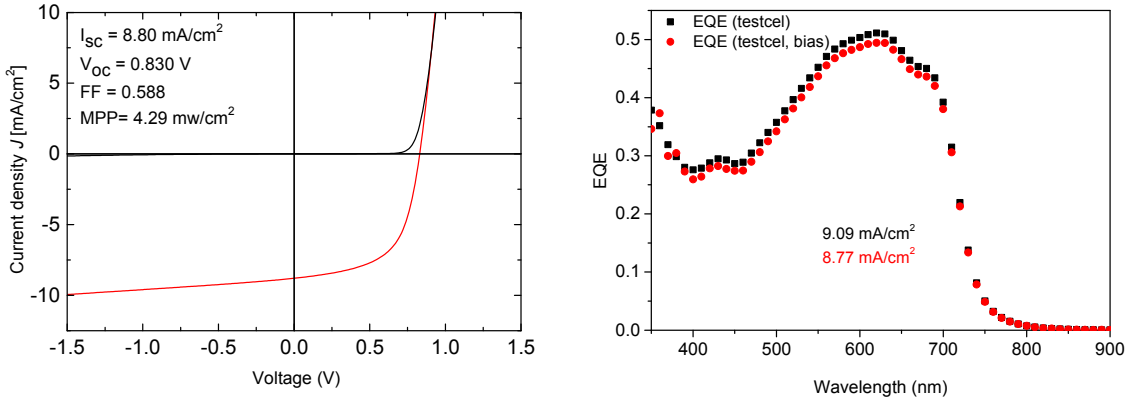

Fig. S7 BDT-EH-S:[60]PCBM *J-V* curve and EQE of optimized device spin coated from $CHCl_3$.

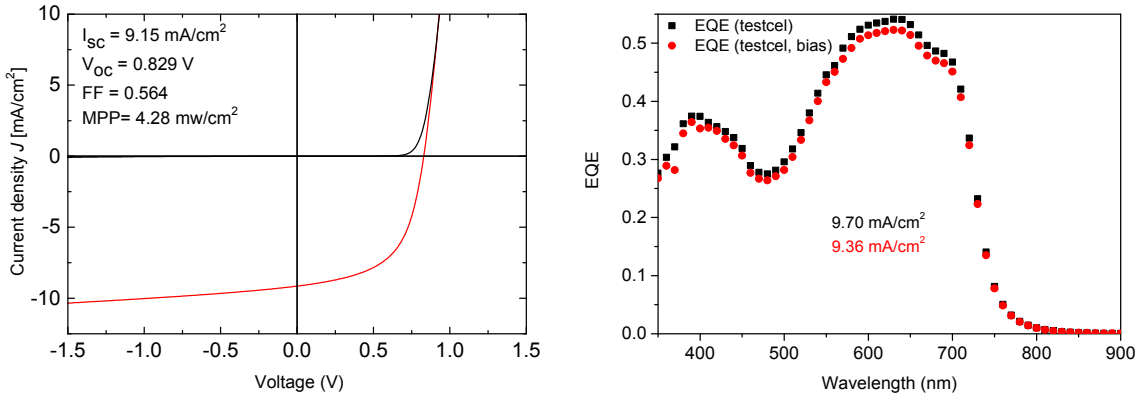

Fig. S8a BDT-EH-S:[60]PCBM *J-V* curve and EQE of optimized device spin coated from 0.2% 1-CN in $CHCl_3$.

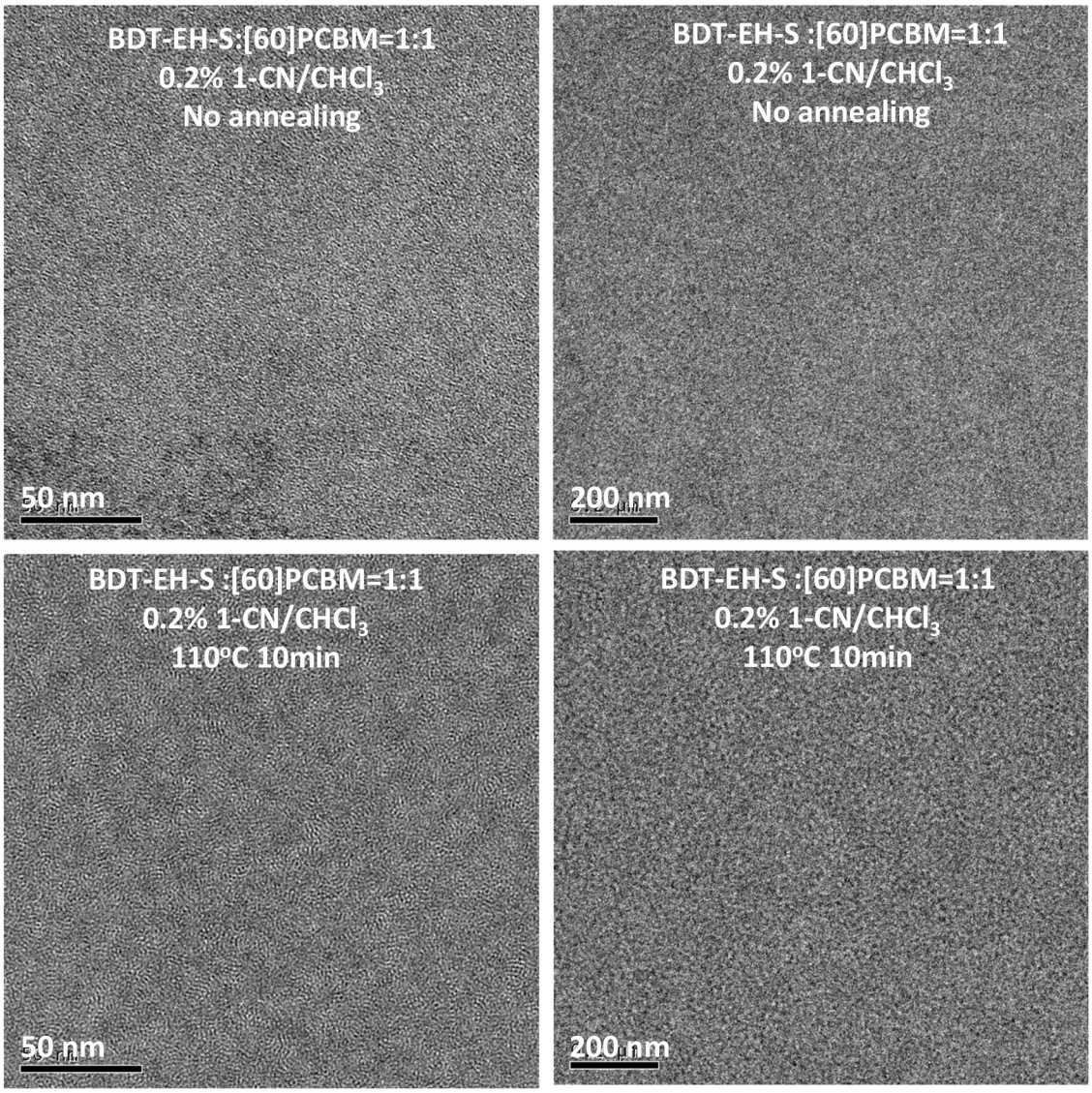

Fig. S8b. TEM images of optimized photoactive layers of BDT-EH-S:[60]PCBM spin coated from 0.2% 1-CN in $CHCl_3$ before and after annealing.

Results for BDT-2C6-S:[60]PCBM

Table S7 Device parameters for BDT-2C6-S:[60]PCBM[a]

D:A	Solvent	Annealing	J_{sc}	V_{oc}	FF	P	$J_{sc,sr}$[b]	PCE
1 : 1	$CHCl_3$	No	4.09	0.951	0.303	1.18		
1 : 1	$CHCl_3$	110 °C 5 min	5.14	0.916	0.318	1.49		
1 : 1	$CHCl_3$	110 °C 10 min	1.48	0.609	0.197	0.18		
1 : 1	0.1% DIO/ $CHCl_3$	No	4.37	0.962	0.315	1.32		
1 : 1	0.2% DIO/ $CHCl_3$	No	5.85	0.923	0.352	1.90		
1 : 1	0.2% DIO/ $CHCl_3$	110 °C 10 min	2.38	0.811	0.241	0.47		
1 : 1	**0.3% DIO/ $CHCl_3$**	**No**	**5.73**	**0.800**	**0.555**	**2.54**	**5.67**	**2.52**
1 : 1	0.2% *o*-DCB/ $CHCl_3$	No	3.72	0.966	0.300	1.08		
1 : 1	0.2% *o*-DCB/ $CHCl_3$	110 °C 10 min	1.72	0.593	0.236	0.24		
1 : 1	0.5% *o*-DCB/ $CHCl_3$	No	3.86	0.957	0.299	1.11		
1 : 1	0.2% 1-CN/ $CHCl_3$	No	3.97	0.974	0.300	1.16	3.59	1.05
1 : 1	0.2% 1-CN/ $CHCl_3$	110 °C 10 min	4.67	0.856	0.285	1.14	2.43	0.59

[a] Units: J_{sc} (mA cm^{-2}), V_{oc} (V), P (mW cm^{-2}), $J_{sc,sr}$ (mA cm^{-2}), and PCE (%).
[b] Current density based on integration of EQE correction, measured with light bias.

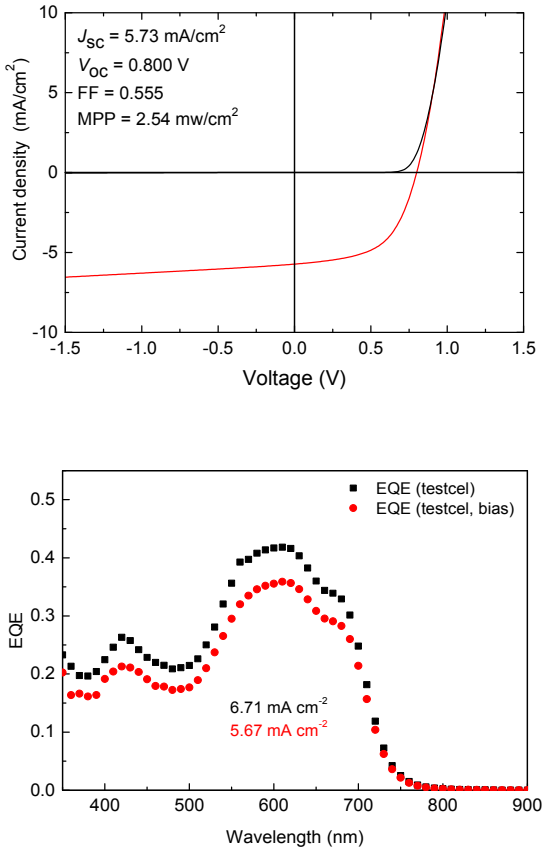

Fig. S9a BDT-2C6-S:[60]PCBM *J-V* curve and EQE of optimized device.

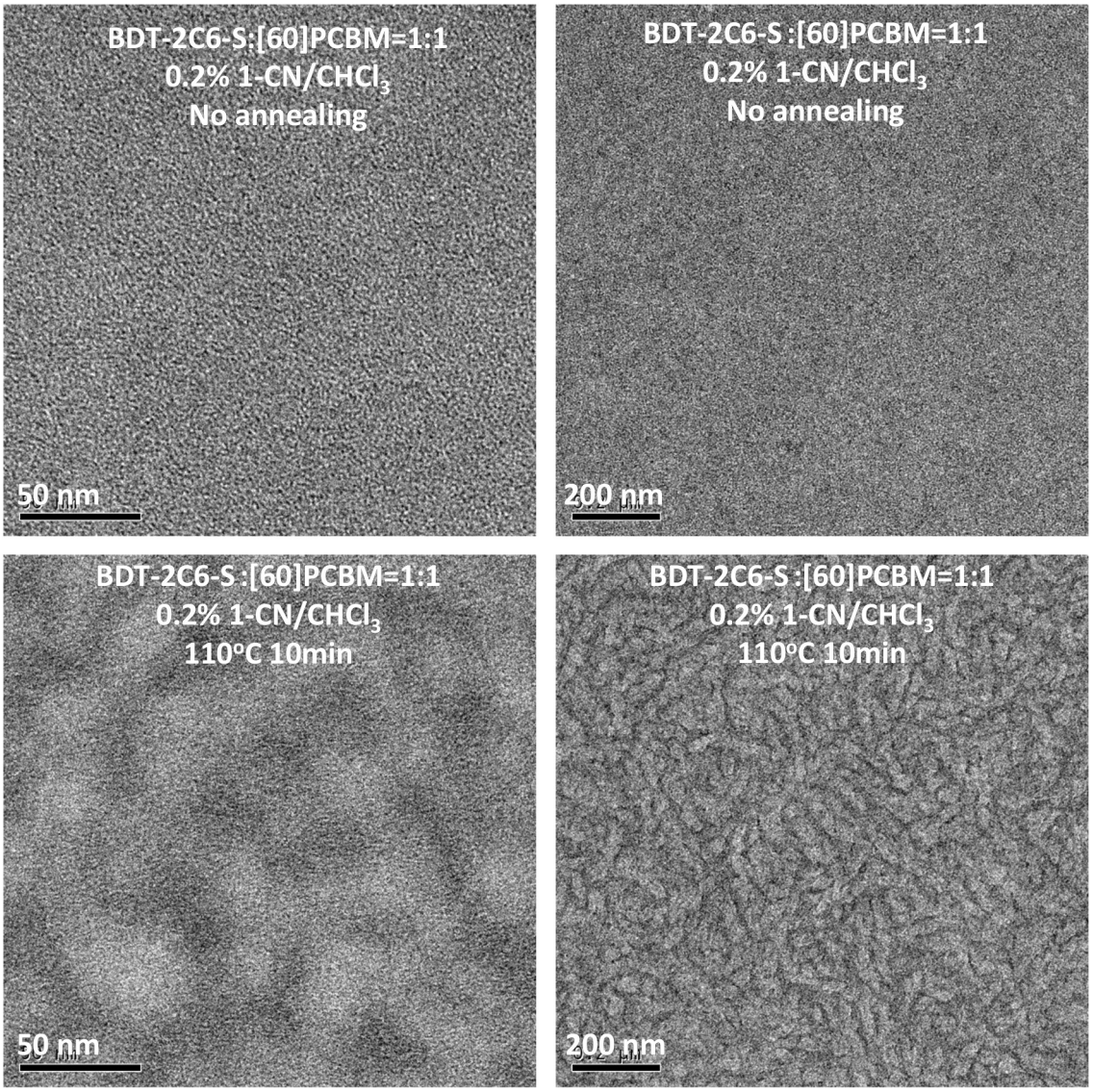

Fig. S9b. TEM images of optimized photoactive layers of BDT-2C6-S:[60]PCBM before and after annealing.

Results for BDT-EH-S-BT:[60]PCBM

Table S8 Device parameters for BDT-EH-S-BT:[60]PCBM[a]

D:A	Solvent	Annealing	J_{sc}	V_{oc}	FF	P	$J_{sc,sr}$[b]	PCE
1 : 1	$CHCl_3$	No	10.80	0.793	0.490	4.22		
1 : 1	**$CHCl_3$**	**110 °C 10 min**	**10.60**	**0.765**	**0.562**	**4.56**	**9.90**	**4.26**
1 : 1	0.2% DIO/ $CHCl_3$	No	9.18	0.739	0.545	3.70		
1 : 1	0.2% DIO/ $CHCl_3$	110 °C 10 min	8.44	0.731	0.485	2.99		
1 : 1	0.2% *o*-DCB/ $CHCl_3$	No	7.93	0.740	0.564	3.31		
1 : 1	0.2% *o*-DCB/ $CHCl_3$	110 °C 10 min	8.99	0.758	0.593	4.04		
1 : 1	0.2% 1-CN/ $CHCl_3$	No	10.00	0.802	0.498	4.01	9.00	3.59
1 : 1	0.2% 1-CN/ $CHCl_3$	110 °C 10 min	9.59	0.777	0.578	4.31	8.88	3.99
3 : 2	$CHCl_3$	No	9.25	0.811	0.420	3.15		
2 : 3	$CHCl_3$	No	11.70	0.776	0.508	4.62	9.88	3.89
2 : 3	$CHCl_3$	110 °C 10 min	10.60	0.792	0.537	4.52	8.99	3.82
2 : 3	0.1% DIO/ $CHCl_3$	110 °C 10 min	10.80	0.780	0.539	4.55	8.08	3.40
2 : 3	0.3% DIO/ $CHCl_3$	110 °C 10 min	11.50	0.776	0.551	4.93	9.47	4.05
2 : 3	0.5% DIO/ $CHCl_3$	110 °C 10 min	8.57	0.737	0.576	3.64		
2 : 3	0.5% *o*-DCB/ $CHCl_3$	110 °C 10 min	10.50	0.774	0.549	4.46		

[a] Units: J_{sc} (mA cm^{-2}), V_{oc} (V), P (mW cm^{-2}), $J_{sc,sr}$ (mA cm^{-2}), and PCE (%).
[b] Current density based on integration of EQE correction, measured with light bias.

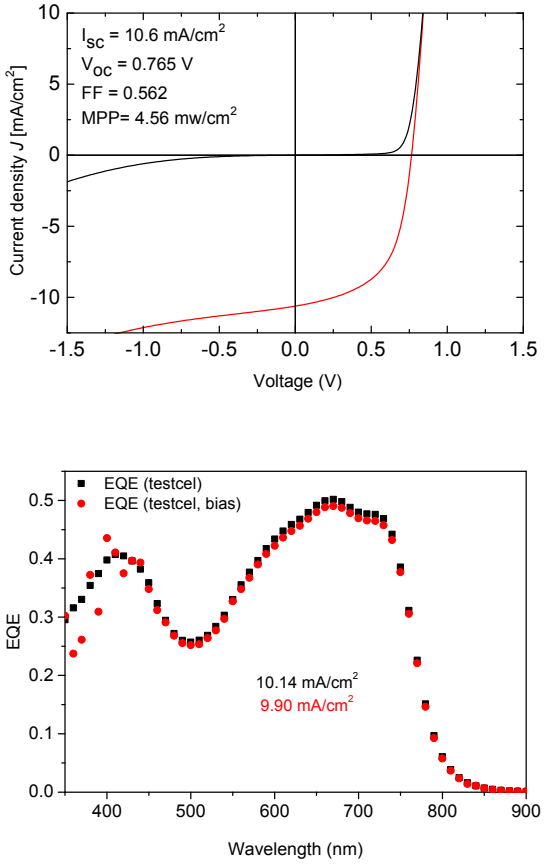

Fig. S10a BDT-EH-S-BT:[60]PCBM *J-V* curve and EQE of optimized device.

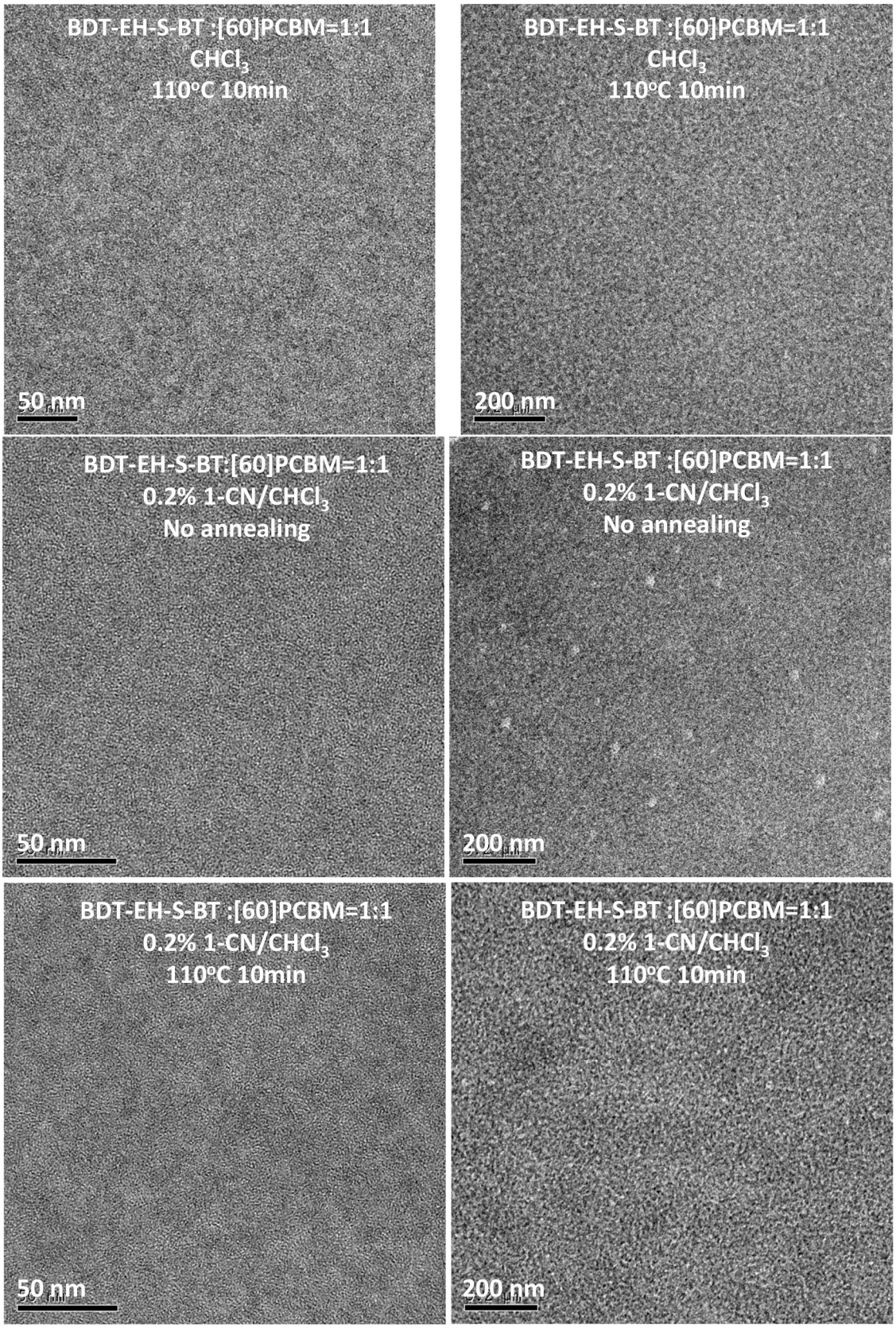

Fig. S10b. TEM images of optimized photoactive layers of BDT-EH-S-BT:[60]PCBM before and after annealing.

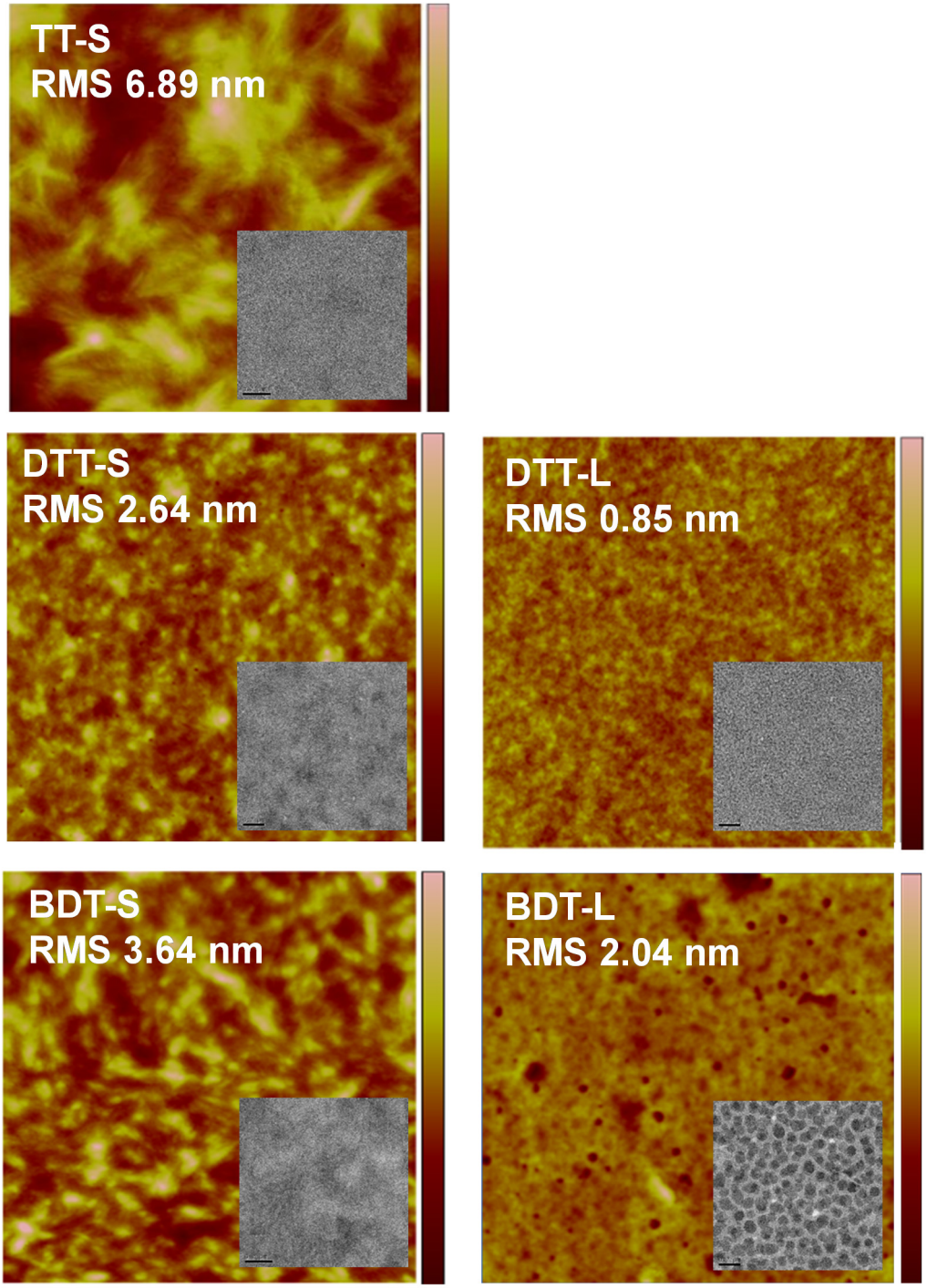

Fig. S11a TEM and AFM height images of optimized photoactive layers of TT-S:[60]PCBM, DTT-S:[60]PCBM, BDT-S:[60]PCBM, DTT-L:[60]PCBM, and BDT-L:[60]PCBM. The size of the AFM scan area is 3 μm × 3 μm and TEM images are on the same magnification. The height scale in the AFM is 30 nm, except for TT-S:[60]PCBM (50 nm) and DTT-L:[60]PCBM (15 nm). The RMS roughness values determined by AFM are given in the insets.

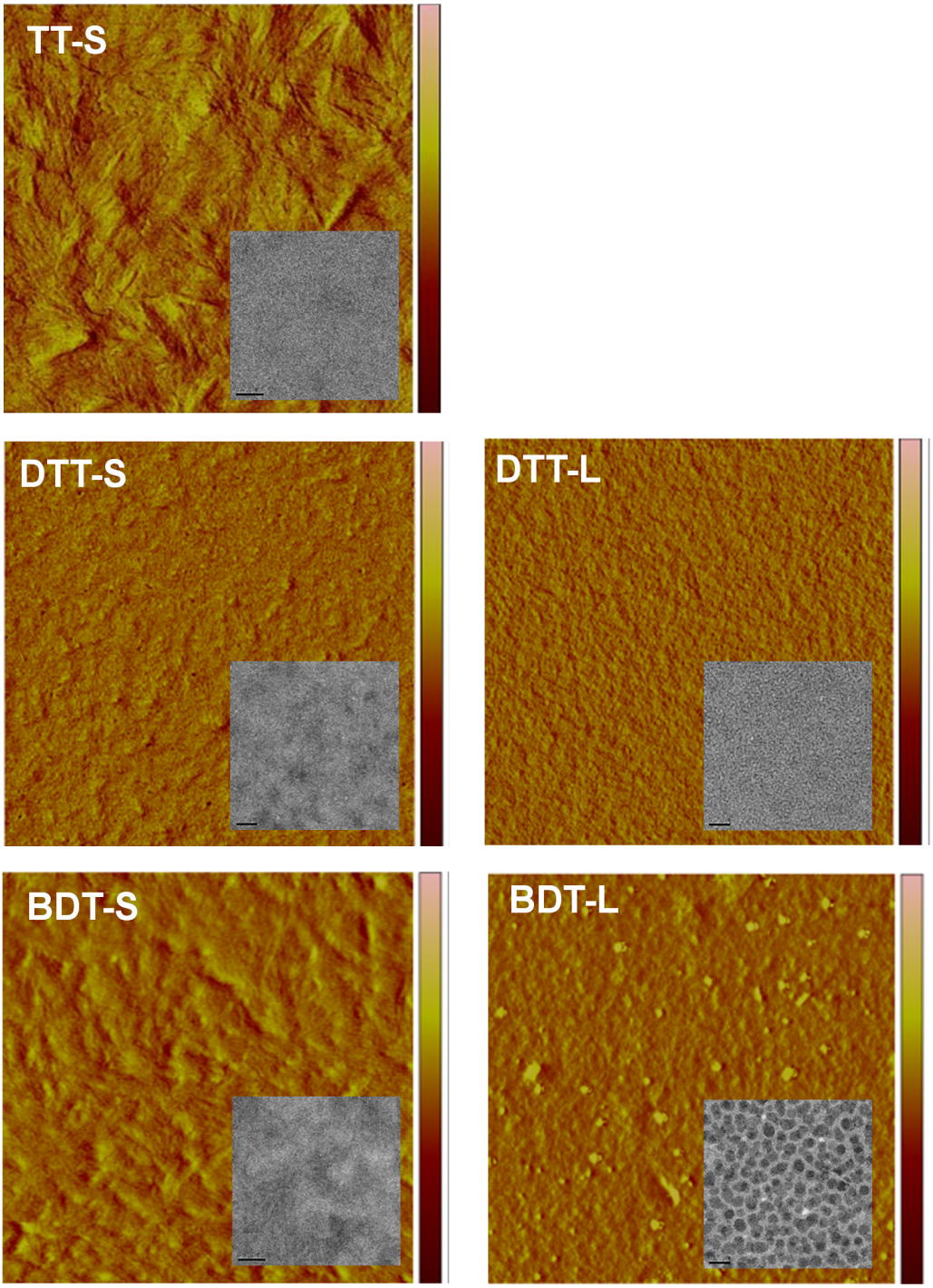

Fig. S11b TEM and AFM phase images of optimized photoactive layers of TT-S:[60]PCBM, DTT-S:[60]PCBM, BDT-S:[60]PCBM, DTT-L:[60]PCBM, and BDT-L:[60]PCBM. The size of the AFM scan area is 3 μm × 3 μm and TEM images are on the same magnification. The height scale is 30 deg., except for TT-S:[60]PCBM (20 deg.) and BDT-L:[60]PCBM (60 deg.).

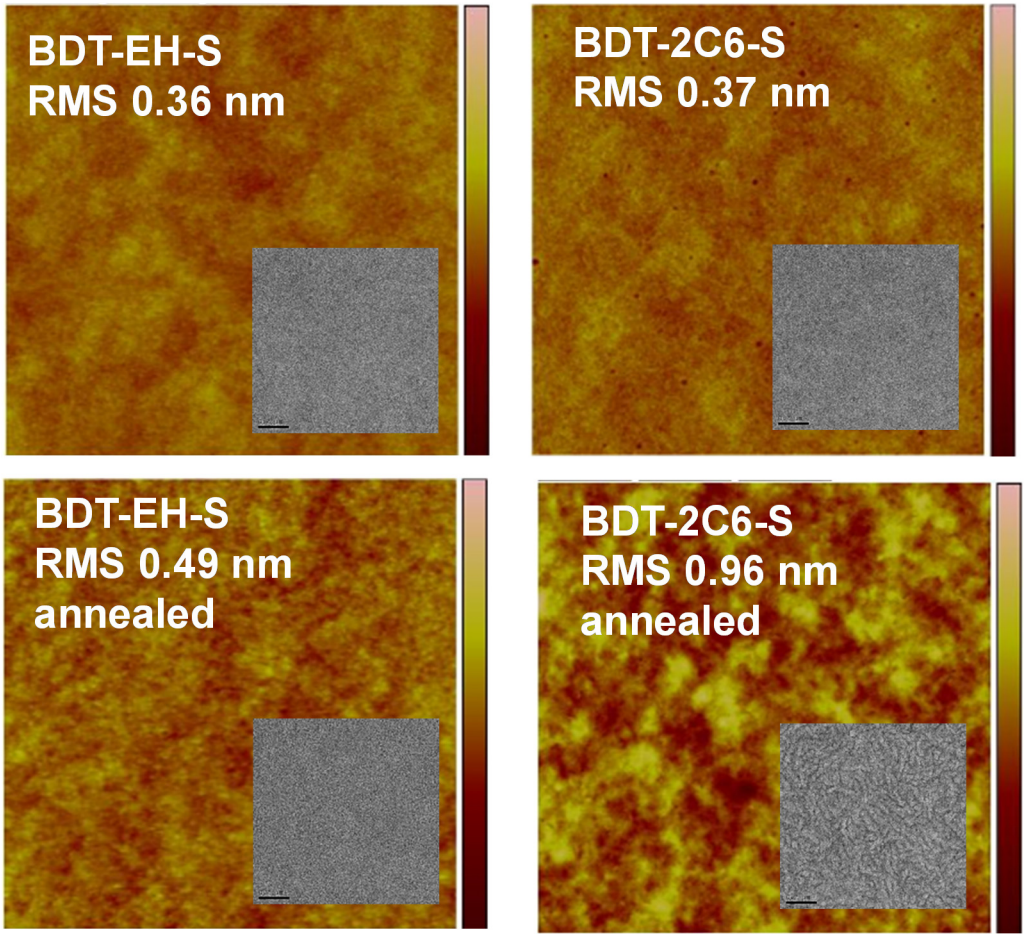

Fig. S12a TEM and AFM height images of optimized photoactive layers of BDT-EH-S (left) and BDT-2C6-S (right) spin coated from chloroform containing 0.2% 1-CN before (top) and after (bottom) thermal annealing at 110 °C for 10 min. The size of the AFM scan area is 3 μm × 3 μm and TEM images are on the same magnification. The height scale in the AFM is 10 nm. The RMS roughness values determined by AFM are given in the insets.

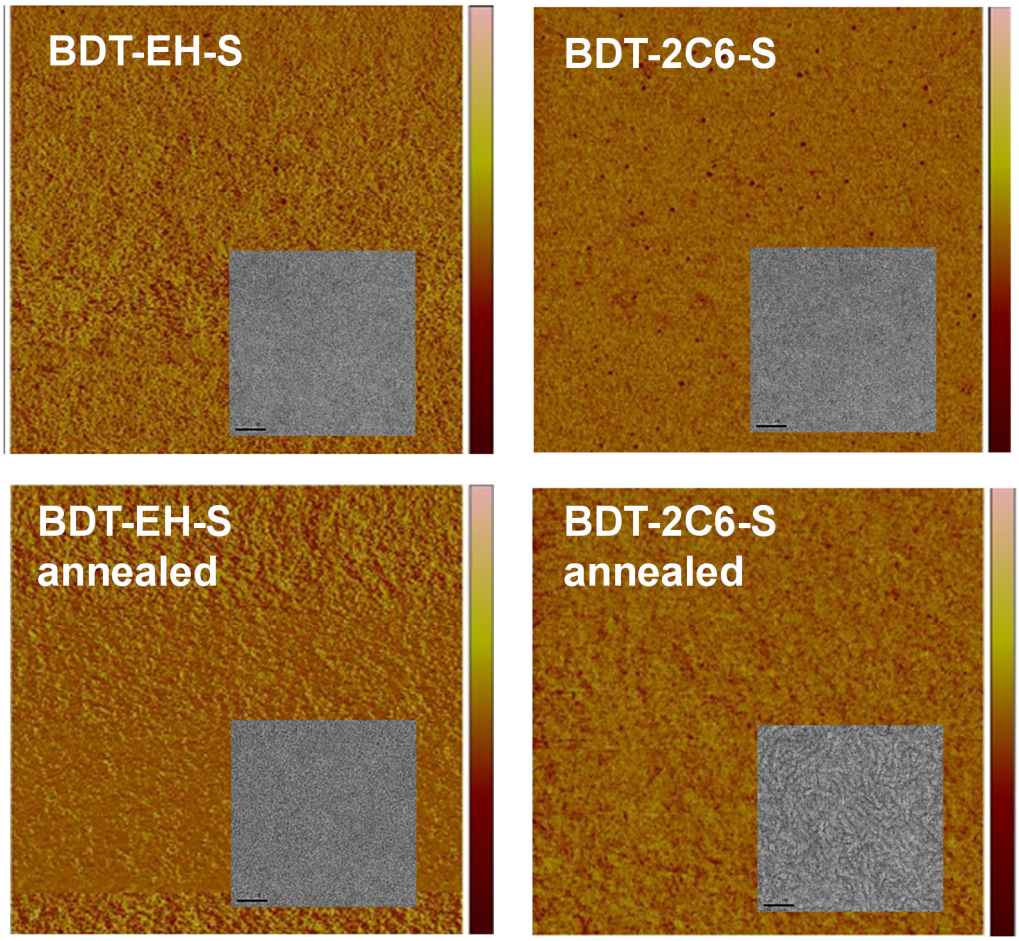

Fig. S12b TEM and AFM phase images of optimized photoactive layers of BDT-EH-S (left) and BDT-2C6-S (right) spin coated from chloroform containing 0.2% 1-CN before (top) and after (bottom) thermal annealing at 110 °C for 10 min. The size of the AFM scan area is 3 μm × 3 μm and TEM images are on the same magnification. The height scale is 50 deg. for BDT-EH-S (left) and 30 deg. for BDT-2C6-S (right).

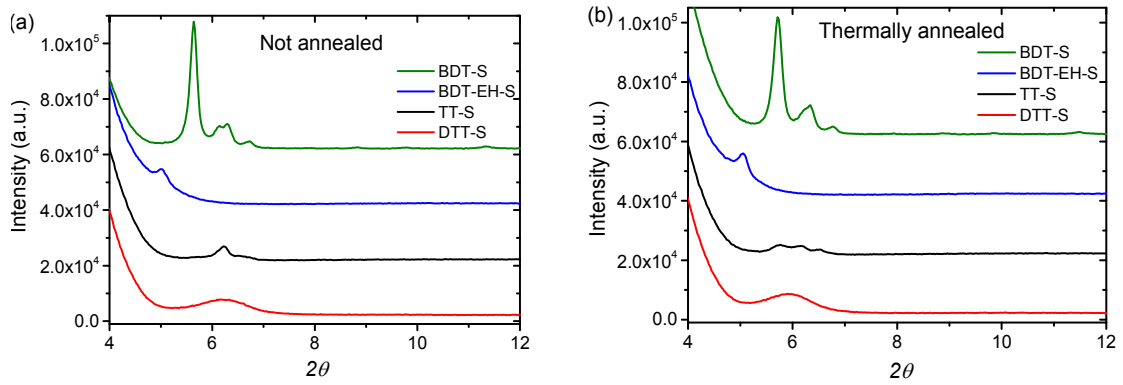

Fig. S13 X-ray diffraction patterns of drop cast films of BDT-S, BDT-EH-S, TT-S, DTT-S before (a) and after (b) thermal annealing.

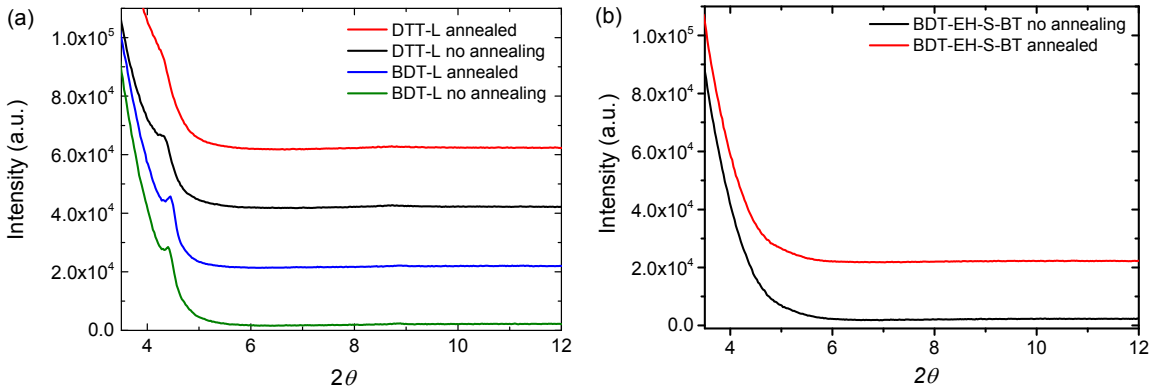

Fig. S14 X-ray diffraction patterns of drop cast films of (a) DTT-L and BDT-L, and (b) BDT-EH-S-BT before and after thermal annealing.

---

[1] K. H. Hendriks, G. H. L. Heintges, V. S. Gevaerts, M. M. Wienk and R. A. J. Janssen, *Angew. Chem. Int. Ed.* 2013, **52**, 8341 –8344.

[2] W. Li, M. Kelchtermans, M. M. Wienk and R. A. J. Janssen, *J. Mater. Chem. A*, 2013, **1**, 15150–15157.